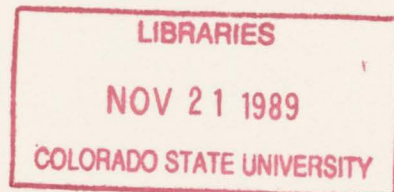


QC852
.C6
no 456
ATSL

**THE GEOMETRICAL, OPTICAL AND
RADIATIVE PROPERTIES OF CIRRUS
CLOUDS**



by G. M. Abakumova, P. P. Anikin, T. V. Yevnevich, E. M. Feigelson, I. A. Gozchakova, L. V. Kravets, Ye. I. Nezval', A. G. Petrushin, T. A. Tarasova and T. A. Tochilkina

**Colorado
State
University**

**DEPARTMENT OF
ATMOSPHERIC SCIENCE**

PAPER NO.

456

THE GEOMETRICAL, OPTICAL AND RADIATIVE PROPERTIES OF CIRRUS CLOUDS

by G. M. Abakumova,¹ P. P. Anikin,² T. V. Yevnevich,¹ E. M. Feigelson,²
I. A. Gorchakova,² L. V. Kravets,¹ Ye. I. Nezval',¹ A. G. Petrushin,³ T.
A. Tarasova² and T. A. Tochilkina¹

Atmospheric Science Bluebook No. 456

October, 1989

¹Geography Department, Moscow State University

²Institute of Atmospheric Physics, Moscow

³Institute Experimental Meteorology, Obninsk

CONTENTS

1 Spectral transmission and optical thicknesses	3
1.1 Experimental device	3
1.2 Results of the experiment	3
2 Studies of the Characteristics of Cirrus Clouds by a Ground-Based Lidar	11
3 Emissivity	19
4 Solar Radiation in Different Sections of the Spectrum According to Data of Ground-Based Measurements	25
4.1 Direct solar radiation	25
4.2 Diffuse and global radiation	27
5 Integral Thermal Radiation Fluxes in Cirrus Clouds	33
6 Optical Models, Calculation of Solar Radiation Fluxes and Radiation Balance	43
6.1 Optical Properties of Crystals	43
6.2 The Radiation Phase Function and the Assymetry Factor of the Phase Function	44
6.3 Albedo of Single Scattering	47
6.4 Calculation of Fluxes Based on Experimental Data	49
6.5 Radiation Balance for Solar and Thermal Radiation	54
7 Conclusion	58

QC852
 C6
 no. 456
 ATSL

LIST OF FIGURES

1.1	The spectral dependence of optical thicknesses $\tau_\lambda/\tau_{\lambda_0}$ for $\lambda_0 = 10.2 \mu m$ for the cirrus cloud of May 22, 1987.	5
1.2	The ratio of optical thicknesses $\frac{\bar{\tau}_\lambda}{\tau_\lambda}$ as a function of the effective radius of particles for the receiver's different angles of view α (1; 15 minutes, 2; 1 degree, 3; 2 degrees, 4; 3 degrees, 5; 4 degrees, 6; 6 degrees, 7; 8 degrees, 8; 10 degrees).	6
1.3	Correlation between measured optical thicknesses τ_{act} and $\tau = 10.2$ for various days during the 1987 experiment.	7
1.4	Spectral transmission of the cirrus cloud in the direction towards the zenith (P_λ^0) as a function of time t during a half-hour interval 13:30-14:00 on May 22, 1987.	7
1.5	Histograms of the recurrence frequencies $N(P_\lambda^0)$ of the transmission of the cirrus cloud in the direction towards the zenith during a half-hour interval of 13:30-14:00 on May 22, 1987.	8
1.6	Histograms of the recurrence frequencies of the transmission of the cirrus cloud in the direction towards the zenith $N(P_\lambda^0)$ during individual years 1986 and 1987 and during the 1978-1987 period.	8
2.1	The restored of the profile of the scattering coefficient MSL in the numerical experiment for 1) prescribed distribution of $\beta\Delta Z$, $\tau = 1.3$, $\gamma\pi = \text{const}$; 2) $\tau = 1.3$, $\gamma\pi = 0.07-0.04 Z/H$; 3) $\tau = 1$, $\gamma\pi = \text{const}$; 4) $\tau = 1$, $\gamma\pi = 0.07-0.04 Z/H$	15
2.2	Histograms of the heights of the lower boundary Z_b (1 and 2) and thicknesses of clouds - H (3 and 4). 1 and 3 for May 1986, 2 and 4 for May 1987.	16
2.3	The average profile of the distribution of the volume scattering coefficient $\beta(Z)$ measurements for clouds with thicknesses near 1 km and a lower boundary between 7.5 and 9 km.	17
2.4	Dependence of the average value of the scattering coefficient $\langle \beta \rangle$ on the thickness of the cloud H for clouds with the lower boundary in the height interval of 7.5-9 km.	17
3.1	Histograms of emittance during the experiment. Solid line - results of 1986; Dashed line - results of 1987.	20
3.2	Effect of the temperature at the lower boundary of the cloud on emissivity.	22
4.1	Recurrence of different values of the optical thickness of high clouds in different regions of the spectrum.	28
4.2	Global radiation in different regions	30

4.3	Recurrence of the global radiation transmission through a solid high cloud cover the ratio of the cloudless sky in different regions of the spectrum during the 1986-1987 experiment periods.	31
6.1	Phase function of visible radiation $\lambda = 0.63 \mu m$ by a system of hexagonal prisms with gamma-distribution in lengths ($\ell_m = 200, C = 4$).	45
6.2	C_Q value for observation periods indicated in Tables 6.1 and 6.3. This value is calculated for two models giving the minimum and maximum values: I and IV.	53
6.3	Value C_A with different albedos of the surface (solid curves - $A_S = 0.1$, dashed curves - $A_S = 0.2$) for two models giving the maximum and minimum values: II and III.	55

PREFACE

THE GEOMETRICAL, OPTICAL AND RADIATIVE PROPERTIES OF CIRRUS CLOUDS

The Department of Atmospheric Science at Colorado State University is pleased to provide a medium for dissemination of results from an experiment studying cirrus clouds conducted in the USSR in 1986-87. The experiment was conducted at the Zvenigorod Scientific Station of the Institute of Atmospheric Physics (USSR Academy of Sciences). The Zvenigorod cloud experiment is the Soviet counterpart of the US FIRE cirrus experiment. This report containing results by Soviet investigators is an important component of the international scientific study of Cloud/Radiation effects on Global Climate. The scientific questions surrounding Clouds/Radiation/Climate, and the consequences of their answers, are truly global in scope and demand the combined effort of the international scientific community. It is in this spirit that Dr. Feigelson of the Institute of Atmospheric Physics, and I have collaborated to bring the important Soviet results summarized in this report to the attention of the American scientific community. We share the hope that this exchange of ideas and knowledge will grow into full collaboration among our US and USSR scientific colleagues.

Stephen K. Cox
Department of Atmospheric Science
Colorado State University
Fort Collins, CO 80523

INTRODUCTION

In May 1986-1987 the Zvenigorod scientific station (ZSS) of the Institute of Atmospheric Physics (USSR Academy of Sciences) conducted a comprehensive ground-gased experiment in studying the optical and radiation properties of cirrus clouds. Scientific leader of the project is Ye. M. Feigelson. Organizer of experimentation is P. P. Anikin.

The following measurements were made:

1. Spectral transmission of solar radiation (IAP).
2. Levels of the boundaries and the vertical profile of the backscattering coefficient (CAO).
3. Emittance in the "window" of 8-12 μm (MIMI).
4. Fluxes of spectral and integral solar radiation – direct, scattered and integrated (MSU).
5. Temperature and humidity near the surface (IAP); full moisture content and estimates of clouds' ice reserve (MIMI).
6. Use was made of aerological probing data in the town of Dolgoprudny lying 80 km away from the town of Zvenigorod.

Theoretical studies and calculations of radiation fluxes were based on experimental data (IAP, IEM). The results of experimental and theoretical studies, along with reviews of the climatology, microphysics and optics of cirrus clouds, are given fully in the collection "Radiative Properties of Cirrus Clouds." Edited by E. M. Feigelson, Nauka Publishers, Moscow, 1989.

LIST OF ABBREVIATIONS

1. IAP - Institute of Atmospheric Physics (USSR Academy of Sciences).
2. ZSS - Zvenigorod Scientific Station of IAP.
3. IEM - Institute of Experimental Meteorology (USSR State Committee for Hydrometeorology and Environmental Control).
4. MSU - Moscow State University (USSR State Committee for Public Education).
5. MIMI - Moscow Instrument - Making Institute (USSR State Committee for Public Education).
6. CAO - Central Aerological Observatory (USSR State Committee for Hydrometeorology and Environmental Control).

Chapter 1

SPECTRAL TRANSMISSION AND OPTICAL THICKNESSES

1.1 Experimental device

The main difficulty of measuring spectral transmission (P_λ) of cirrus clouds in natural conditions is due to their great spatial and temporal variability. Bearing this in mind, to measure P_λ use was made of an optical device which made it possible to carry out simultaneous measurements of P_λ in five sections of the spectrum in the range $\lambda = 0.3-12 \mu m$ 1) $0.3 - 0.5 \mu m$; 2) $0.32 - 0.8 \mu m$; 3) $0.4 - 1.2 \mu m$; 4) $0.5 - 2.2 \mu m$; 5) $2 - 12 \mu m$]. To determine P_λ in the above sections of the spectrum the values of the intensity of radiation (I_λ) were recorded simultaneously by five self-recorders of the KSP-4 type. The value I_λ was recorded with the resolution with respect to the spectrum: $\Delta\lambda = 1 \cdot 10^{-3} \mu m$ when $\lambda = 0.3; 0.6; 1.2 \mu m$ and $\Delta\lambda = 4 \cdot 10^{-2} \mu m$ when $\lambda = 3.9$ and $10.2 \mu m$. The opportunity of recording I_λ continuously with respect to the spectrum in any of its five sections was envisaged. The solar radiation flux into the device was directed by a special Sun tracking unit situated at a height of 15m. The bulk of the luminous flux was directed into the measuring channel of the two-beam spectrophotometer UR-20 tuned in to $\lambda = 10.2 \mu m$. Using a system of mirrors and semitransparent quartz plates, a portion of the flux was directed on spectrometers DMR-4; MDR-2; SPM-2 (two instruments) which were tuned in to $\lambda - 0.31; 0.63; 1.2; 2.1; 10.2 \mu m$. The angle of view of the device was about 15 minutes. The device is described in detail by Anikin P., *et al.*, (1981).

1.2 Results of the experiment

The spectral transmission P_λ of cirrus clouds was determined from the following relation:

$$P_\lambda = I_\lambda / I_\lambda^0 \quad (1)$$

where I_λ and I_λ^o are relative values of the intensity of direct solar radiation which passed through clouds and in breaks between them.

Then the transparency and optical thickness in the direction towards the zenith was determined: $P_\lambda^o = P_\lambda^{COS\theta}$; $\tau_\lambda = -\ln P_\lambda^o$, where θ is the sun's zenith angle. The initial values of I_λ in the range $\tau = 0 - 2$ were determined with the casual relative error of 5% which is mainly due to the inaccuracy in detecting the 100% line (i.e., transmission when the sky is clear). As a rule, the 100% line is determined before and after the passage of the cloud. Such an interpolation is most suitable for clouds which have frequently occurring breaks. An error is also possible due to not sharply pronounced breaks (barely discernible clouds) and due to the instability of the operation of instrumentation during a day.

During the 1986-1987 experiment, the data of P_λ^o measuring the $\lambda = 10.2 \mu m$ region were mainly processed. In the UV and visible spectral regions, along with the useful signal (i.e, direct solar light), a portion of scattered light (the greater portion the lower λ is) can get into the radiation receiver with a small angle of view, due to the sharply pronounced elongated shape of the indicatrix of large crystals in cirrus clouds. As a result, the measured value of P_λ increases while τ_λ decreases. Figure 1.1 gives the spectral dependence of $\tau_\lambda/\tau_{\lambda_0}$ for $\lambda_0 = 10.2 \mu m$ obtained on May 22, 1987. We have calculated this effect for models of ice spherical particles with different effective radii in the wavelength range $\lambda = 0.6-10 \mu m$ at the receiver's angles of view (α) ranging from 15 minutes to 10 degrees. The results of calculations are presented in Figure 1.2. Here $\bar{\tau}$ is the optical thickness of the cloud with the contribution of scattered radiation getting into the angle of the receiver's opening. τ is the same for true direct radiation. It follows from Figure 1.2 that in the visible range of the spectrum even at $\alpha = 15$ minutes for large particles the value $\bar{\tau}/\tau$ is much smaller than 1. With the growth of λ the deviation of $\bar{\tau}/\tau$ from unity with the same size of particles becomes smaller, which indicates the decrease of the share of scattered radiation in the measured signal. With $\lambda = 10 \mu m$, $\bar{\tau}/\tau = 1$ in the entire range of particle sizes of interest for us. This was the main cause of the selection of the wavelength $\lambda = 10.2 \mu m$ in determining τ . The measured value of τ directly corresponds to emittance measured in the transparency window of 8-12 μm :

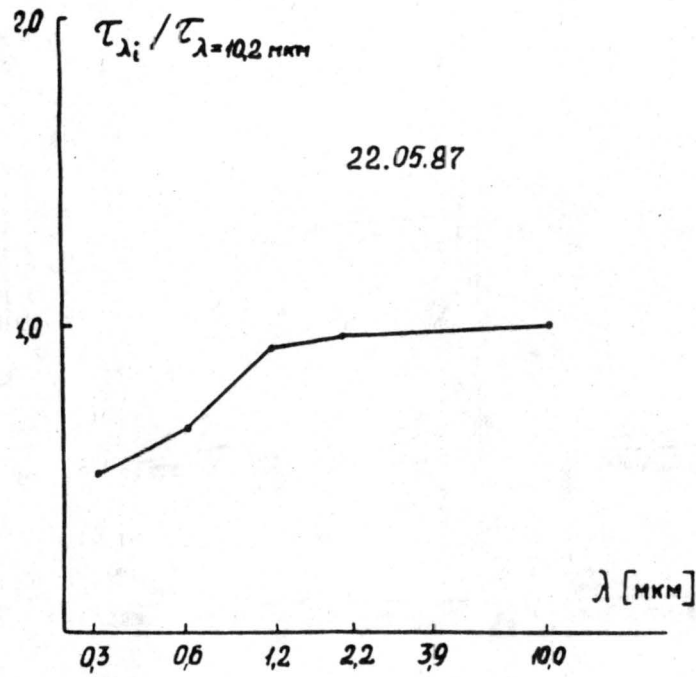


Figure 1.1: The spectral dependence of optical thicknesses $\tau_{\lambda}/\tau_{\lambda_0}$ for $\lambda_0 = 10.2 \mu m$ for the cirrus cloud of May 22, 1987.

$$\epsilon = 1 - e^{-\tau} \quad (2)$$

Finally, ignoring in the present stage of theoretical studies (see below) the effect of small particles, it can be assumed for solar and thermal radiation that:

$$\tau_{\lambda} = const = \tau_{\lambda_0}, \lambda_0 = 10 \mu m. \quad (3)$$

The comparison of measured data by an integral actinometer with the angle of view $\delta = 10$ degrees and our installation ($\delta = 15$ minutes) when $\lambda = 10.2 \mu m$ is a convincing confirmation of the data of Figure 1.2 and equalities (3). Figure 1.3 presents the results of simultaneous measurements. The ratio $\bar{\tau}/\tau = 0.5$ obtained from calculations is fulfilled practically exactly: $\tau_{act} \approx 0.5 \tau_{\lambda} (\lambda = 10.2 \mu m)$. Figure 1.4 shows $P_{\lambda}^{\circ} (\lambda = 10.2) \mu m$ as a function of time obtained after treatment on a computer (the curve is drawn through points plotted after equal intervals $\Delta t = 1$ min) during the experiment conducted on May 22, 1987 (13:30-14:00). The average value of $P_{\lambda}^{\circ} (10.2 \mu m)$ during 0.5 hr = 0.63. Figure 1.5 shows the frequency of the recurrence of values of $P_{\lambda}^{\circ} (10.2 \mu m)$ during the same period.

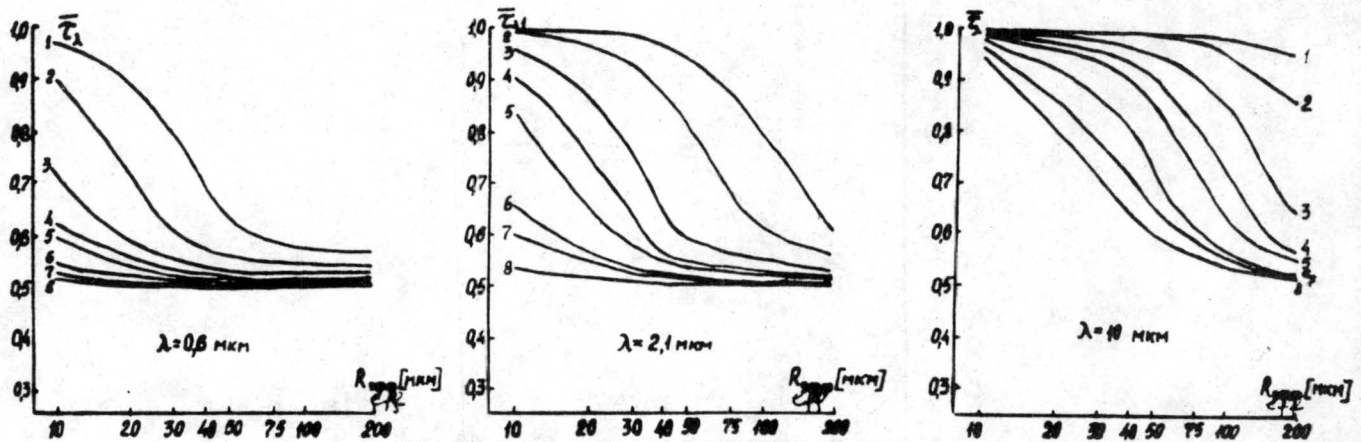


Figure 1.2: The ratio of optical thicknesses $\frac{\bar{\tau}_\lambda}{\tau_\lambda}$ as a function of the effective radius of particles for the receiver's different angles of view α (1; 15 minutes, 2; 1 degree, 3; 2 degrees, 4; 3 degrees, 5; 4 degrees, 6; 6 degrees, 7; 8 degrees, 8; 10 degrees).

Histograms of the recurrence of values P_λ^o ($10.2 \mu m$) for cirrus clouds during individual years of the experiment, as well as the averaged histogram for the 1978-1987 period are given in Figure 1.6 and in Table 1.1. The overall time of observations is 89 hours. Table 1.2 gives accumulated recurrence frequencies of the values P_λ^o of $\lambda = 10.2 \mu m$ during individual days of measurements in the 1986-1987 period. Table 1.3 summarizes average values of $P_\lambda^o(\lambda = 10.2 \mu m)$ during half-hour intervals. Table 1.4 lists average values of $P_\lambda^o(\lambda = 10.2 \mu m)$ for a day, dispersions (σ^2) and time intervals Δt during which autocorrelation coefficients ≥ 0.7 . It is evident from the figures and tables that cirrus clouds observed at the Zvenigorod scientific station are mainly thin semitransparent clouds. Apparently the predominance of thin C_i is typical of the region under study which is confirmed by the measurements of the 1978-1987 period during various seasons.

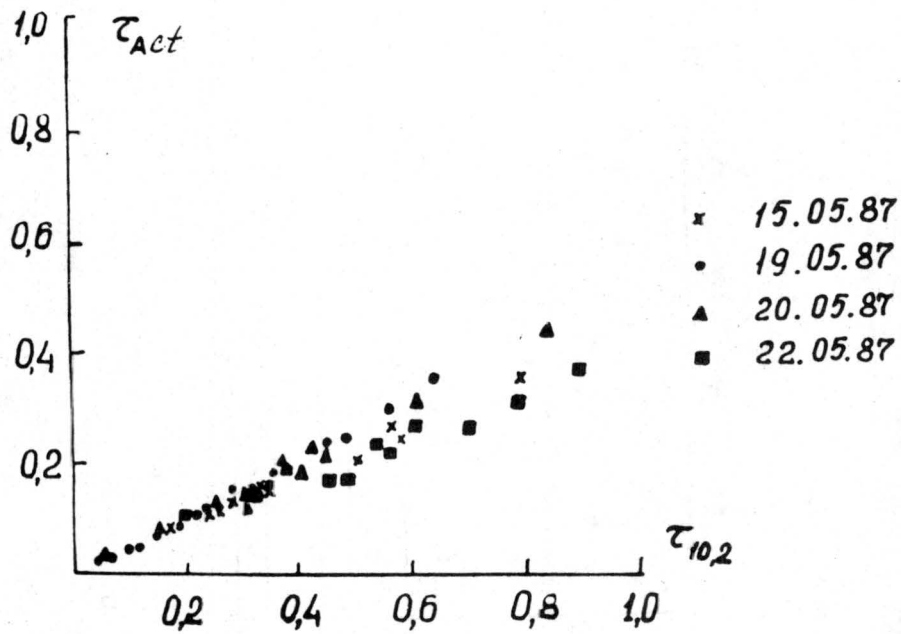


Figure 1.3: Correlation between measured optical thicknesses τ_{act} and $\tau = 10.2$ for various days during the 1987 experiment.

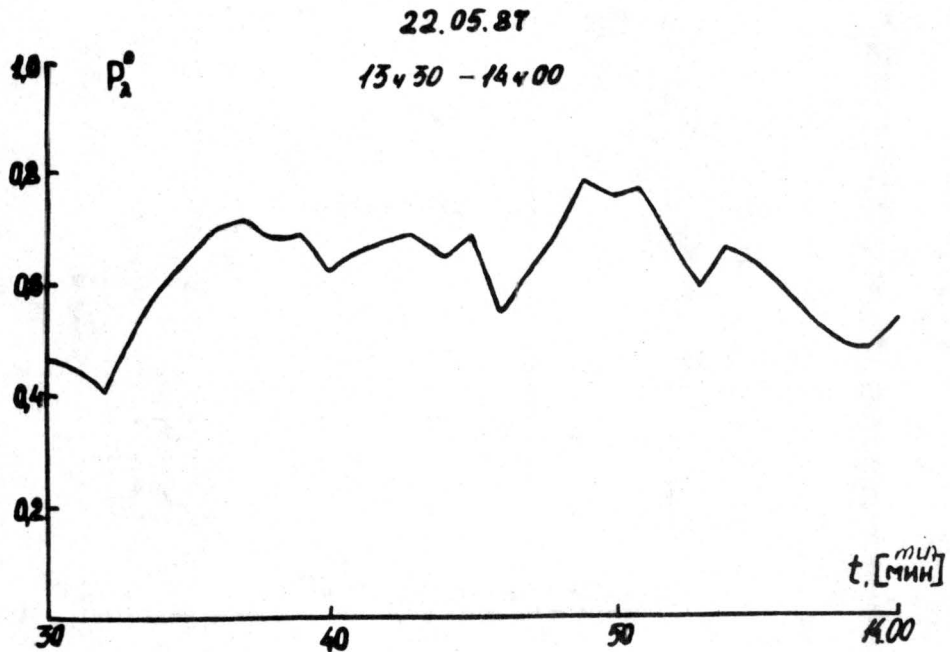


Figure 1.4: Spectral transmission of the cirrus cloud in the direction towards the zenith (P_{λ}°) as a function of time t during a half-hour interval 13:30-14:00 on May 22, 1987.

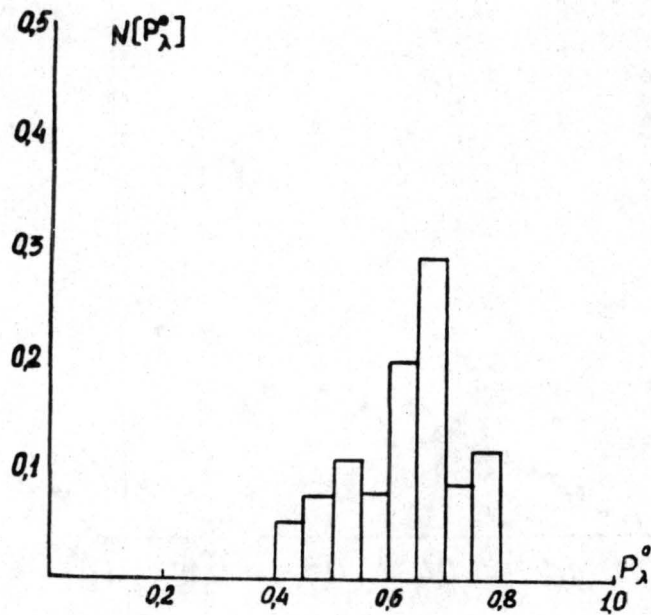


Figure 1.5: Histograms of the recurrence frequencies $N(P_\lambda^0)$ of the transmission of the cirrus cloud in the direction towards the zenith during a half-hour interval of 13:30-14:00 on May 22, 1987.

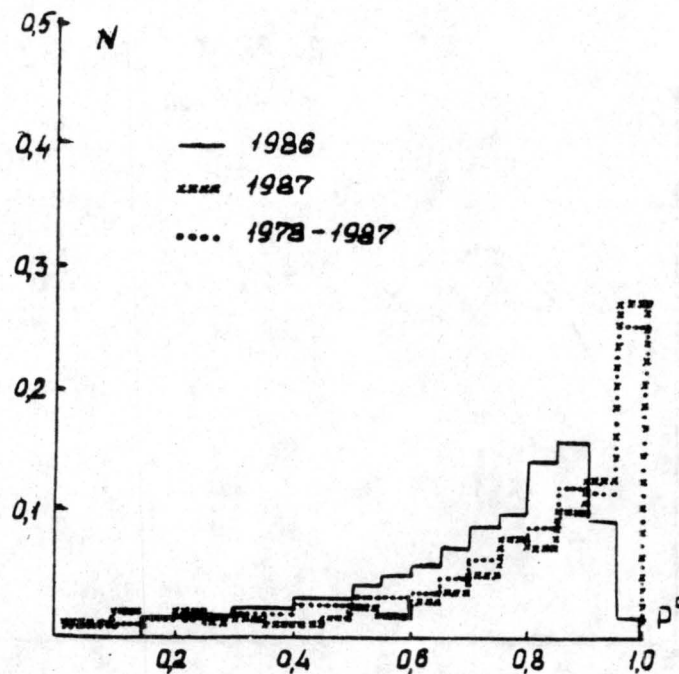


Figure 1.6: Histograms of the recurrence frequencies of the transmission of the cirrus cloud in the direction towards the zenith $N(P_\lambda^0)$ during individual years 1986 and 1987 and during the 1978-1987 period.

Table 1.1. Yearly histograms for P°

	1978	1979	1980	1981	1985	1986	1987	1978-1987
1.00 - 0.95	0.192	0.414	0.420	0.359	0.141	0.015	0.285	0.261
0.95 - 0.90	0.097	0.101	0.130	0.181	0.096	0.097	0.129	0.119
0.90 - 0.85	0.092	0.119	0.114	0.113	0.152	0.163	0.103	0.123
0.85 - 0.80	0.108	0.086	0.062	0.066	0.084	0.146	0.082	0.091
0.80 - 0.75	0.123	0.048	0.105	0.067	0.068	0.103	0.082	0.085
0.75 - 0.70	0.087	0.039	0.078	0.050	0.047	0.092	0.065	0.065
0.70 - 0.65	0.058	0.030	0.028	0.044	0.032	0.072	0.053	0.045
0.65 - 0.60	0.054	0.018	0.010	0.031	0.034	0.059	0.037	0.036
0.60 - 0.55	0.047	0.042	0.002	0.020	0.035	0.051	0.018	0.031
0.55 - 0.50	0.027	0.046	0.034	0.015	0.040	0.042	0.023	0.032
0.50 - 0.45	0.015	0.023	0.017	0.016	0.041	0.031	0.016	0.023
0.45 - 0.40	0.016	0.016	0	0.024	0.052	0.031	0.012	0.022
0.40 - 0.35	0.016	0.011	0	0.005	0.042	0.026	0.011	0.016
0.35 - 0.30	0.017	0.005	0	0.002	0.036	0.026	0.016	0.015
0.30 - 0.25	0.013	0.001	0	0.003	0.028	0.017	0.013	0.011
0.25 - 0.20	0.010	0.001	0	0.002	0.022	0.014	0.019	0.010
0.20 - 0.15	0.014	0	0	0.002	0.019	0.014	0.015	0.009
0.15 - 0.10	0.011	0	0	0	0.016	0.001	0.019	0.006
0.10 - 0.05	0.002	0	0	0	0.014	0	0.001	0
0.05 - 0.00	0	0	0	0	0.001	0	0.001	0

Table 1.2. Accumulated frequencies of P° for separate days.

Time/Day	11.05.86	24.05.86	4.05.87	6.05.87	15.05.87	19.05.87	20.05.87	22.05.87
1 - 0.95	0	0.029	0.680	0.110	0.266	0.395	0.061	0.213
1 - 0.90	0.152	0.071	0.924	0.244	0.290	0.561	0.143	0.347
1 - 0.85	0.446	0.106	0.974	0.415	0.312	0.670	0.326	0.427
1 - 0.80	0.711	0.137	0.995	0.560	0.319	0.740	0.456	0.541
1 - 0.75	0.837	0.217	1.000	0.779	0.339	0.786	0.578	0.618
1 - 0.70	0.922	0.315	1.000	0.924	0.352	0.815	0.711	0.688
1 - 0.65	0.978	0.402	1.000	0.962	0.357	0.853	0.806	0.828
1 - 0.60	0.997	0.500	1.000	0.999	0.371	0.882	0.870	0.907
1 - 0.55	1.000	0.599	1.000	1.000	0.403	0.910	0.882	0.937
1 - 0.50	1.000	0.684	1.000	1.000	0.472	0.938	0.895	0.967
1 - 0.45	1.000	0.746	1.000	1.000	0.521	0.957	0.906	0.986
1 - 0.40	1.000	0.808	1.000	1.000	0.553	0.972	0.918	1.000
1 - 0.35	1.000	0.860	1.000	1.000	0.575	0.994	0.934	1.000
1 - 0.30	1.000	0.911	1.000	1.000	0.656	0.997	0.951	1.000
1 - 0.25	1.000	0.941	1.000	1.000	0.722	0.999	0.962	1.000
1 - 0.20	1.000	0.970	1.000	1.000	0.818	1.000	0.979	1.000
1 - 0.15	1.000	0.997	1.000	1.000	0.894	1.000	0.991	1.000
1 - 0.10	1.000	1.000	1.000	1.000	1.000	1.000	0.995	1.000
1 - 0.05	1.000	1.000	1.000	1.000	1.000	1.000	1.000	1.000
1 - 0.00	1.000	1.000	1.000	1.000	1.000	1.000	0.998	1.000

Table 1.3. Mean values of P for 30 minute intervals for different days.

Time/Day	11.05.86	24.05.86	4.05.87	6.05.87	15.05.87	19.05.87	20.05.87	22.05.87
8:30- 9:00					0.884			
9:00- 9:30					0.307			
9:30-10:00					0.426			
10:00-10:30		0.723				0.884	0.828	
10:30-11:00		0.666					0.841	
11:00-11:30		0.707					0.840	
11:30-12:00		0.604					0.846	
12:00-12:30		0.711					0.601	0.886
12:30-13:00		0.844					0.626	0.941
13:00-13:30		0.661		0.891			0.519	
13:30-14:00		0.471		0.762				0.630
14:00-14:30	0.764		0.972			0.793	0.815	0.727
14:30-15:00	0.848	0.379	0.958			0.963		
15:00-15:30		0.315	0.931			0.996		
15:30-16:00		0.662	0.902			0.935		
16:00-16:30	0.919	0.584	0.974			0.956		
16:30-17:00	0.887		0.978			0.965		
17:00-17:30	0.838		0.989			0.927		
17:30-18:00	0.736		0.951			0.716		
18:00-18:30			0.941			0.785		
18:30-19:00						0.535		
19:00-19:30						0.826		

Table 1.4. Mean values of P° for whole days; dispersions - δ_p^2 and time intervals of autocorrelation coefficients being not less than 0.7.

	11.05	24.05	4.05	6.05	15.05	19.05	20.05	22.05
	1986				1987			
$\overline{P}_{10.2}^\circ$	0.83	0.64	0.95	0.83	0.54	0.85	0.74	0.80
δ_p^2	0.002	0.018	0.001	0.005	0.043	0.011	0.020	0.007
Δt (sec)	55	90	17	65	140	72	120	120

Chapter 2

STUDIES OF THE CHARACTERISTICS OF CIRRUS CLOUDS BY A GROUND-BASED LIDAR

The lidar designed at the CAO consists of a transmitter and a receiver/detector directed toward the zenith. The transmitter uses a neodymium glass laser with a doubled radiation frequency. During the experiment the lidar operated with the receiver and the transmitter separated from each other by 4 m. The receiver's angle of view was roughly equal to the divergence angle of the transmitter's beam (3 mrad). The function describing the intersection of the directional patterns of the receiver and the transmitter depending on height was determined experimentally. For this purpose the altitude profile of the Raman signal of atmospheric nitrogen (N_2) in the night-time was recorded and compared with the height distribution of N_2 concentration. Table 2.1 lists the main parameters of the lidar used and the parameters of the lidar described in [Platt *et al.*, 1987].

Table 2.1. Lidar Parameters

	Wave-length	Pulse energy	Pulse duration	Transmitter's angle	Receiver's angle	Aerial diameter
COA lidar (glass +Nd)	1060nm 503nm	10J 1.5J	30ns	3mrad	3mrad	50cm
Lidar Platt <i>et al.</i>	694 nm	1J	60ns	2mrad	5mrad	30cm

The lidar's high energy potential enabled the reliable recording of cirrus clouds at any time of the day. The lidar helped to solve two problems:

1. Determination of the heights of cloud boundaries.
2. Restoration of the vertical profile of the scattering coefficient, $\beta(Z)$, for $\lambda = 530$ nm.

Cloud boundaries were determined from the threshold values of the backscattering

coefficient $\beta_{\pi, min}(Z)$. The boundary values of $\beta_{\pi}(Z)$ are obtained by comparing measured signals from cirrus clouds with signatures of aerosol and molecular scattering and the daytime sky background entering recording instrumentation. The values of $\beta_{\pi}(Z)$ taken as boundaries of thin cirrus clouds are listed in Table 2.2.

Table 2.2. Boundary values of $\beta_{\pi, min}(km^{-1})$ as a function of the height H of their detection.

Height	$\lambda_1 = 1060nm$	$\lambda_2 = 530nm$
6-7 km	$2 \cdot 10^{-3}$	$5 \cdot 10^{-3}$
8-9 km	$3 \cdot 10^{-3}$	$7.5 \cdot 10^{-3}$
10-11 km	$4 \cdot 10^{-3}$	10^{-2}

Work with this lidar has shown that the accuracy of determining the boundaries of cirrus clouds during measurements in the daytime is higher for $\lambda_1 = 1060$ nm.

This method of determining the boundaries of thin clouds is conventional. Aerosol fluctuations and, correspondingly, the aerosol backscattering coefficient greater than those taken as boundary ones for clouds are possible. Nevertheless, as a rule, cirrus clouds with the optical thickness $\tau < 0.1$ have values β_{π} which exceed the boundary values by a factor of 10 or more. This enables the differentiation of them from aerosol layers. In determining the upper boundary of optically thick clouds it is necessary to take into account multiple scattering and the attenuation of the signal along the path in the cloud. Therefore, in daytime conditions the minimally detected value of $\beta_{\pi}(Z)$ corresponding to the upper boundary will increase with the growth of τ . Correspondingly in such measurements we shall observe the trend of the error in the level of the upper boundary towards its decrease, if one uses the values of Table 2.2. To restore the profiles of the scattering coefficient of the cloud from the measured profile of the lidar echo signal the solution of the inverse problem is needed. Within the framework of the designation adopted the lidar equation may be written as:

$$S(Z) = A \cdot Z^{-2} \cdot \beta_{\pi} \cdot \exp(-2 \int_0^Z \beta(Z') dz'). \quad (1)$$

$S(Z)$ is the signal received from the elementary volume lying at the height Z and A is the instrumentation function.

We have worked out the technique which includes, in addition to the measurements of the profile of the signal $S(Z)$, the measurements of the coefficient of directed transmission into the zenith of the entire cloud T_o .

The technique is based on a modified method of successive layers MSL. The method requires the knowledge of the ratio of signals from adjacent layers. On the sounding route, the MSL method gives a recursive equation for values $\beta(\Delta Z_i)$ and $\beta(\Delta Z_{i+1})$ for neighboring layers ΔZ_i and ΔZ_{i+1} [Zuyev V. Ye., *et al.*, 1976]:

$$\beta(\Delta Z_{i+1}) = \beta(\Delta Z_i) \cdot T^{-2}(\Delta Z_i) \cdot \frac{S(\Delta Z_{i+1})}{S(\Delta Z_i)} \quad (2)$$

where $T^2(\Delta Z_i) = \exp(-2\beta(\Delta Z_i) \cdot \Delta Z_i)$

In deriving (2) a slight change in height of the indicatrix¹ γ_π in the cloud is expected compared with the change of $\beta(Z)$. Let us note that in (2) the parameter A , the determination of which involves difficulties, is excluded. In the presence of the altitude profile of $S(Z)$, correspondingly $S(\Delta Z_i)$, $i = 1, \dots, N$ and the measured coefficient of the directed transmission of the cloud we propose the following algorithm of calculating the function $\beta(Z)$:

1. a certain value of $\beta(\Delta Z_k)$ for the k th layer is given a priori when $1 < K < N$ (the layer K is chosen closer to the upper boundary so that the value would be large enough, which leads to a smaller error.
2. according to formula (2) the profile $\beta(\Delta Z_i)$ is calculated. Then a comparison is made of the calculated optical thickness $[\tau = \sum_{i=1}^n \beta(\Delta Z_i) \cdot \Delta Z_i]$ and the logarithms of the measured value of T_o

¹indicatrix - phase function

$$\tau_o = -\ln T_o \quad (3)$$

If the condition $\tau = \tau_o$ is not fulfilled, the value of the parameter $\beta(\Delta Z_k)$ varies, and cycles are repeated before the fulfillment of the last condition. As a result, we obtain the profile of the scattering coefficient $\beta(\Delta Z_i)$.

The numerical experiment carried out in Zuyev V. Ye., *et al.*, (1976) shows that in the entire range of optical thicknesses $\tau < 4$, even at the reception angle $\varphi_d = 1^\circ$, the deviation $\Delta\beta/\beta$ due to the multiple scattering background did not exceed 10%. We have conducted a numerical experiment to determine the effect of the changes of the backscattering indicatrix as a function of height with the cloud upon the accuracy of the restoring $\beta(Z)$. In this experiment we also studied the effect of the error in determining the optical thickness τ on the accuracy of the retrieval of the $\beta(Z)$ profile by the proposed method. Figure 2.1 summarizes the results of restoring the profile by the suggested technique. The range of the change in the indicatrix corresponds to the experimentally obtained values (Sassen, K., 1978; Wendling, P., and Wendling, R., 1979). In the numerical experiment, the indicatrix varied with the height of the cloud according to the linear law $\gamma_\pi(Z) = 0.07 - 0.04Z/H$.

As evident from Figure 2.1, the inaccuracy in optical thickness τ is more critical than the change of γ_π when reconstructing the $\beta(Z)$ profile. The graph shows that with a 30% error in determining τ and with γ_π varying within boundary limits, the qualitative character of the function $\beta(Z)$ is traced and that for the greater part, the prescribed cloud quantitative coincidences are accurate enough. With smaller values of τ the influence of the variability of the indicatrix on the accuracy of the reconstruction of $\beta(Z)$ decreases. According to calculations for $\tau = 0.13$ the profile $\beta(Z)$ with the linearly varying indicatrix differs from the prescribed profile by units of per cent. Thus, the suggested technique makes it possible to reliably reconstruct the profiles of the scattering coefficient in cirrus clouds. The practical value of the method consists in using only experimental information for solving eq. (1). Besides, the calibration of the lidar is not needed.

For the practical implementation of the above method in the daytime, use was made of the lidar measurements of the profile of the return signal and data on the value τ_λ for $\lambda = 10.2 \mu m$. (These data were obtained by the photometric method – see section 1).

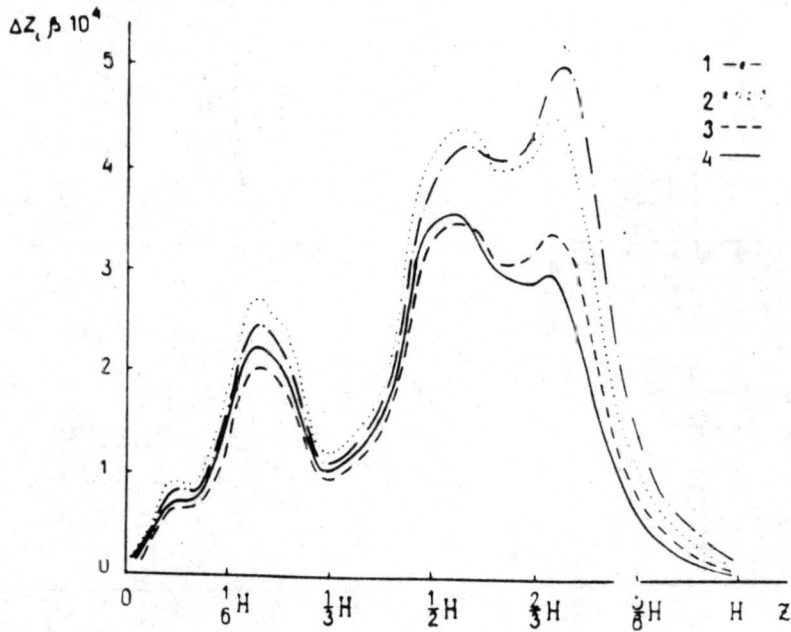


Figure 2.1: The restoration of the profile of the scattering coefficient MSL in the numerical experiment for 1) prescribed distribution of $\beta\Delta Z$, the optical thickness of the cloud $\tau = 1.3$, $\gamma\pi = \text{const}$; 2) $\tau = 1.3$, $\gamma\pi = 0.07-0.04 Z/H$; 3) $\tau = 1$, $\gamma\pi = \text{const}$; 4) $\tau = 1$, $\gamma\pi = 0.07-0.04 Z/H$.

The results given below relate to two cycles of measurements conducted within the framework of complex experiments at the ZSS in May 1986 and May 1987. The measurements were made for all high clouds in the altitude range of 5.5-12 km. The general character of the altitude distribution of high clouds during the experiment is reflected by histograms presented in Figure 2.2. In May 1986 mainly thin cirrus clouds were observed. The average thickness for the entire measuring period was 600 m. In May 1987 thicker high clouds were observed; the average thickness for this period was 1000 m. The optical thicknesses varied within $\tau = 0.1 - 1.2$. In May 1986 the height distribution of the lower boundary of cirrus clouds was relatively uniform in the entire altitude interval while most of cirrus clouds observed in May 1987 consisted of clouds with variations of the lower boundary within 8-9 km.

For the entire population of reconstructed profiles of the scattering coefficient, $\beta(Z)$ it was obtained that, as a rule, the maximum value of $\beta(Z)$ lies within the limits 0.4-1.2 km^{-1} . The absolute maximum of the values of $\beta(Z)$ obtained lay at a height of

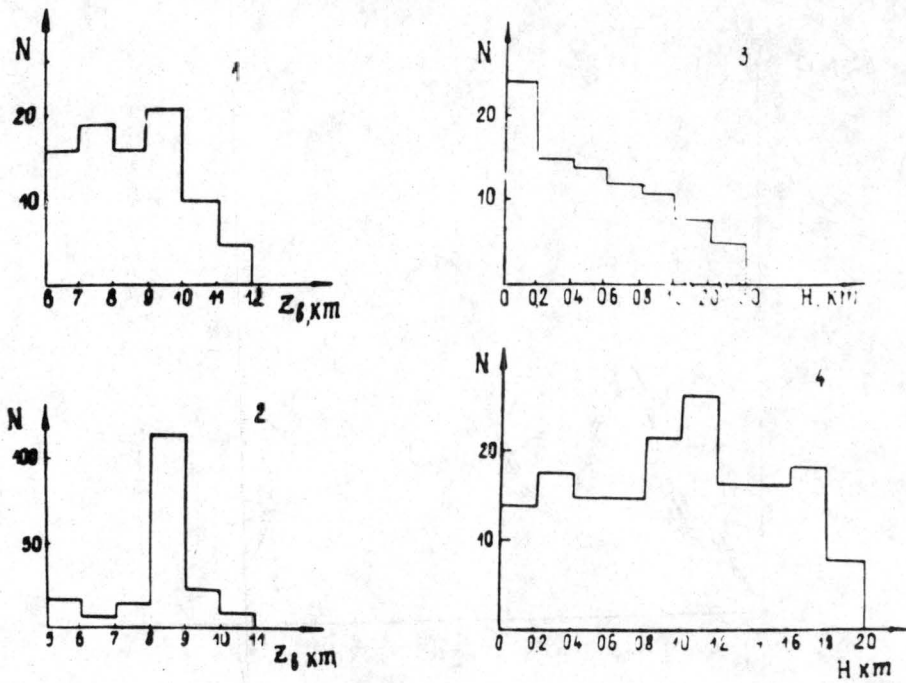


Figure 2.2: Histograms of the heights of the lower boundary Z_b (1 and 2) and thicknesses of clouds - H (3 and 4). 1 and 3 for May 1986, 2 and 4 for May 1987.

6.7 km and was equal to 2.4 km^{-1} . The average in profile values of $\langle \beta(Z) \rangle$ lies within the limits of $0.15\text{-}0.8 \text{ km}^{-1}$. Using the data obtained, we calculated the average relative profile $\beta(Z)$ represented in Figure 2.3 for clouds whose thickness was close to 1 km, for all cases available when the height of the lower boundary lay within 7.5-9 km. It can be concluded that the average profile of the distribution of $\beta(Z)$ in the given height interval has a weakly pronounced dome-shaped maximum slightly shifted towards the upper boundary. "Instantaneous" profiles for which the averaging was carried out had various shapes, including the bimodal shape with maxima near the lower and upper boundaries. The result of comparing the measured thicknesses of cirrus clouds with the scattering coefficient $\langle \beta \rangle$ average for the thickness of the cloud in them is given in Figure 2.4 for clouds whose lower boundary lay within the height interval of 7.5-9 km. It follows from Figure 2.4, that as of the thickness of cirrus clouds increases a decreasing trend towards the average volume scattering coefficient is observed.

The comparison of the thicknesses of observed cirrus clouds with the temperature t_0^o at the height of the middle of the cloud did not lead to obvious regular features.

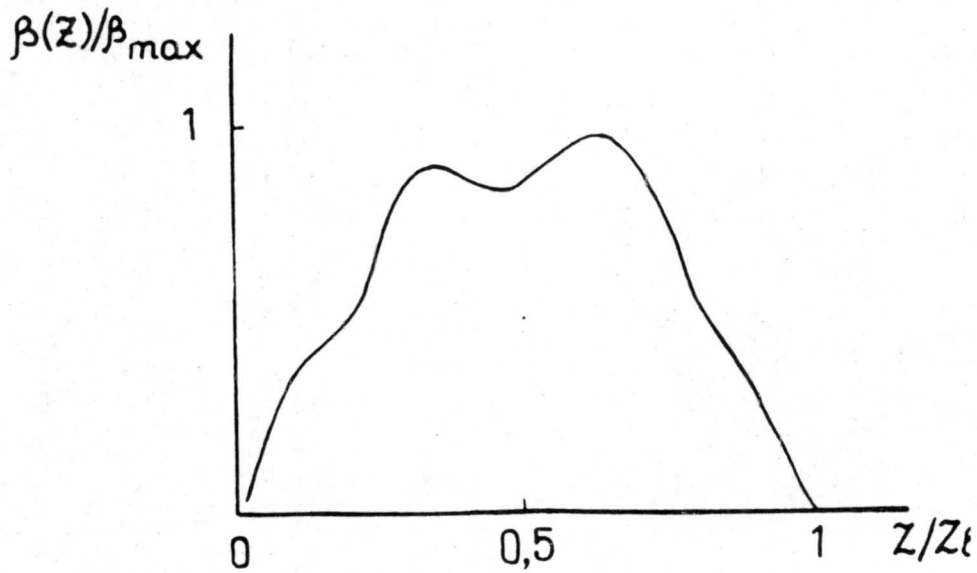


Figure 2.3: The average profile of the distribution of the volume scattering coefficient $\beta(z)$ for the entire cycle of measurements for clouds whose thickness is close to 1 km, and whose lower boundary lies within the limits of 7.5-9 km.

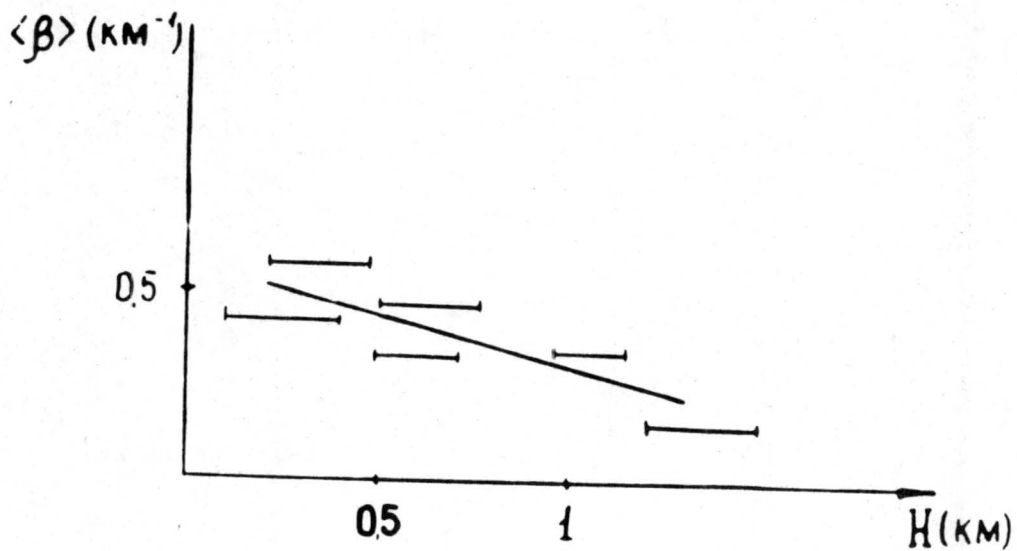


Figure 2.4: Dependence of the average value of the scattering coefficient $\langle \beta \rangle$ on the thickness of the cloud H for clouds with the lower boundary in the height interval of 7.5-9 km.

For instance, in the most statistically significant case the thicknesses of clouds for the temperature interval $45^{\circ}\text{C} < t_o < -40^{\circ}\text{C}$ varied from 0.4 to 1.8 km.

Chapter 3

EMISSIVITY

(Research was directed by Professor Dr. A. G. Gorelik)

The emittance of cirrus clouds was measured by an IR-radiometer which has the following technical characteristics: the spectral range of operation 8-12 μm , the width of the directional pattern 1 degree, sensitivity 0.1° K with the blackbody temperature 283° K and time constant 1 sec. Measurements were conducted in May 1986 and 1987 on the Earth's surface in the direction towards the zenith. The emissivity of cirrus clouds from the data of an IR-radiometer and a lidar was determined according to the formulae (Zhuravlyova, V. A. *et al.*, 1983).

$$\epsilon = \frac{\tau_{cl}}{B(T)} \quad (1)$$

$$\tau_{cl} = \frac{\tau_m - \tau_{uc}}{p} - \tau_r \quad (2)$$

where

- ϵ = emissivity of the cloud,
- $B(T)$ - blackbody emission at the temperature of the lower boundary,
- τ_{cl} - cloud's own emission,
- τ_m - emission measured near the Earth's surface,
- τ_{uc} - emission of the subcloud layer,

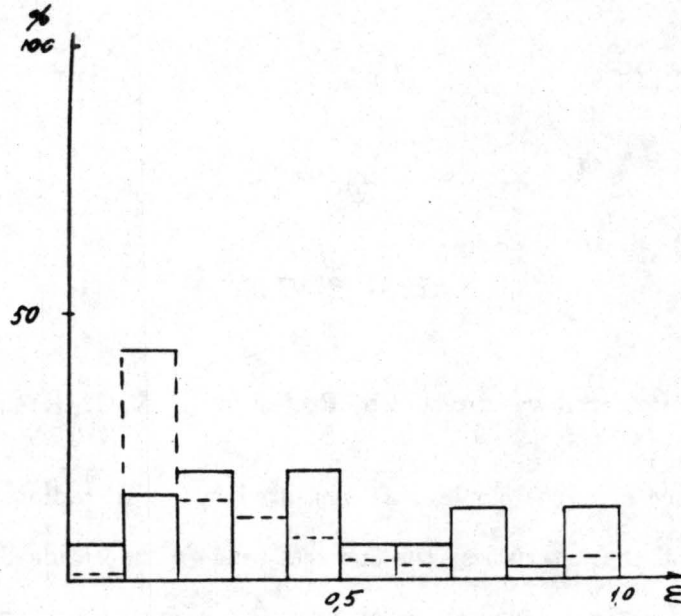


Figure 3.1: Histograms of emittance during the experiment. Solid line - results of 1986; Dashed line - results of 1987.

- τ_r - Earth's emission reflected from the cloud
- p - the transmission of the undercloud layer.

In our case $\tau_m - \tau_{uc}$ is determined as a difference between the emission of the cloudy and the clear sky. We ignore the emission of the above-cloud layer. $B(T)$ is determined on the basis of aerological data and lidar data of the height of the lower boundary.

According to experimental data the emissivity during the period of measurements in 1986 varied from 0.1 to 0.99 and in 1987 from 0.08 to 0.96. Figure 3.1 presents histograms for these periods.

Table 3.1 lists mean values of ϵ , their dispersions (σ_ϵ) and the mean ice content (m_w^z) for different days and hours of measurements.

Table 3.1. Characteristics of cirrus clouds during the given period of measurements.

Date time	Mean emissivity	Dispersion σ_ϵ	Mean ice content g/m^2
10.01.86			
13:00-14:00	0.457	0.0317	47.56
14:00-15:00	0.658	0.0256	61.5
15:00-16:00	0.484	0.0301	52.6
4.05.87			
14:00-15:00	0.371	0.0203	23.3
15:00-16:00	0.25	0.085	12.9
16:00-17:00	0.134	0.04	6.51
17:00-18:00	0.149	0.0122	7.77
19.05.87			
14:30-15:30	0.15	0.01	8.34
15:30-17:30	0.288	0.115	15.81
17:30-18:30	0.263	0.0142	14.57
20.05.87			
11:30-12:30	0.22	0.125	11.88
12:30-13:30	0.234	0.151	13.04
22.05.88			
11:30-12:30	0.297	0.0127	16.6
12:30-13:30	0.26	0.108	14.03

The ice content was determined from the expression;

$$m_w^z = prr_{ct}$$

where

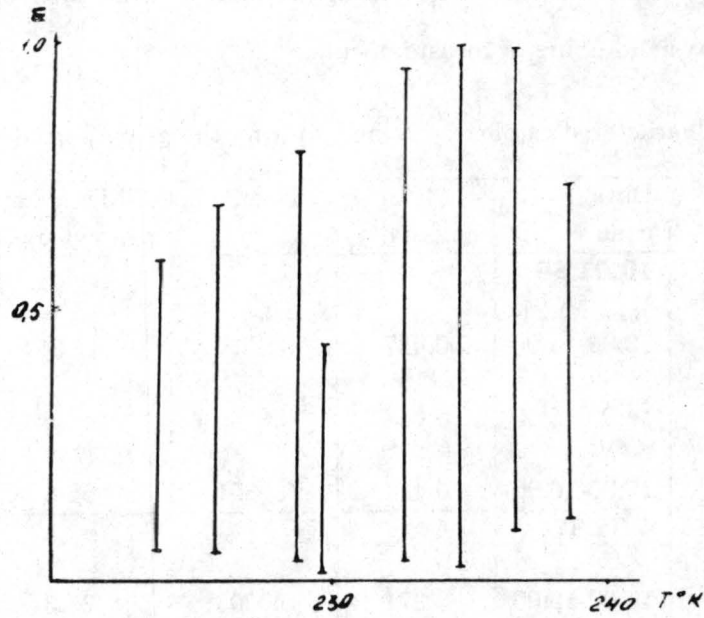


Figure 3.2: Effect of the temperature at the lower boundary of the cloud on emissivity.

$$\tau_{cl} = \ln \frac{1}{1 - \epsilon} \quad (3)$$

- ρ = ice density, 0.9 g/cub m;
- r = effective radius $\approx 50 \mu m$.

The effect of the temperature of air near the cloud bottom on emissivity was estimated from experimental data. The range of variations of emissivity as a function of the temperature is presented in Figure 3.2. It is evident from Figures 3.1 and 3.2 that irrespective of the temperature clouds with $\epsilon = 0.1-0.2$ prevail. With the rise in the temperature the range of the variation of emittance expands.

During the experiment and simultaneously with the operation of the complex in the range of 8-12 μm , spectral radiance at $\lambda = 0.8$ cm and $\lambda = 1.35$ cm was recorded at the surface. The SHF-radiometer has the following technical characteristics: sensitivity via channels with $\lambda = 0.8$ cm is 0.1 deg K, $\lambda = 1.35$ cm is 0.2 deg K, the bandwidth $\lambda = 0.8$ cm is 2 GHz, $\lambda = 1.35$ cm is 500 MHz, the aerial's directional pattern $\lambda = 0.8$ cm is 1.0 deg, and $\lambda = 1.35$ cm is 1.7 deg.

The above-mentioned wavelengths are used for determining the integral moisture content in the atmosphere.

The integral moisture content for the cloudless atmosphere is calculated from radiometric brightness temperatures by the equations of regression [Gorelik, A. G. *et al.*, 1975].

$$T_r^{0.8} = a_1 + b_1 Q$$

$$T_r^{1.35} = a_2 + b_2 Q$$

where $a_1 = 12.8$ $b_1 = 0.69$
 $a_2 = 9.1$ $b_2 = 1.76$
 and Q is the integral moisture (vapor) content.

Table 3.2 lists the values of integral moisture content obtained by equations of regression and from radiosonde sounding observations.

Table 3.2

Date	Time	T of air deg C	Q regression equation	Q sounding
8.05.86	12:00	21.0	14	13.6
10.05.86	14:30	13.5	9	8.4
11.05.86	13:30	11.0	9	8.0
12.05.86	13:20	13.0	10	15.0
13.05.86	10:20	13.5	17	17.8
	13:30	19.0	18	17.2

This method of determining Q requires absolute calibration. At present calibration-free methods of determining the integral moisture content are being worked out.

In the case of cloudiness, the equations of regression are written this way:

$$T_r^{0.8} = a_1 + b_1Q + C_1W$$

(4)

$$T_r^{1.35} = a_2 + b_2Q + C_2W$$

where W is the liquid-water component.

Coefficients C_1 and C_2 are calculated from the data on the temperature of the lower boundary of the cloud.

Equations (4) enable one to divide liquid and vapor moisture and are used for different types of clouds except cirrus.

Table 3.3 summarizes variations of measured values and their mean-square deviations. ΔQ is the variation of the integral moisture content with respect to the clear sky measured in breaks.

The minimal recorded amount of liquid-water moisture is 1 g/sq m. In cirrus clouds ice liquid-water moisture does not exceed this value.

Table 3.3

Date	ΔQ <i>kg/sq m</i>	W <i>g/sq m</i>	σ_w	$\sigma_{\Delta Q}$
8.05.86				
15:25-15:40	0.13-2.6	0.0089-0.06	27.52×10^{-3}	0.749
13.05.86				
14:20-15:30	0.1-6.5	0.005-0.6	152.83×10^{-3}	2.85

Chapter 4

SOLAR RADIATION IN DIFFERENT SECTIONS OF THE SPECTRUM ACCORDING TO DATA OF GROUND-BASED MEASUREMENTS

Direct integral solar radiation was measured by Yu. D. Yanishevsky's thermoelectric actinometer whose angle of view is equal to 10 degrees. The set of wideband light filters made it possible to determine the value of direct radiation in spectral regions $\lambda < 525$ nm, 380-710 nm and $\lambda > 710$ nm.

Global (Q) and diffuse (D) integral radiation (INT) were measured by a thermoelectric pyranometer; photosynthetically active radiation (PAR, 380-710 nm) and near infrared (NIR, $\lambda > 710$ nm) radiation were measured by color GGO pyranometers, while ultraviolet radiation (UV, $\lambda < 380$ nm) was measured by the UV meter of Moscow University. The angle of view of these instruments was 180 degrees. In measurements of diffuse radiation, the devices were shaded from direct solar radiation by a shading screen. The latter was used to exclude the near-solar zone 10 degrees in diameter equal to the actinometer's angle of view. The relative error of measurements by the actinometer was equal to 3% and by other devices to 11%.

When the sky was clear or the cirrus cloud cover was solid, observations of direct and diffuse radiation were conducted in half an hour or greater intervals. Global radiation (INT, PAR, UV) were recorded continuously. $Q_{NIR} = Q_{INT} - Q_{PAR} - Q_{UV}$.

4.1 Direct solar radiation

To assess the influence of high clouds on direct solar radiation (I), cases were chosen when the sun's disk was occluded by clouds. There were 16 such days - ten in 1986 and six in 1987.

To evaluate the effect of cloudiness alone on I, the transmission coefficient (P^o) and optical thickness (τ) of cirrus clouds in the vertical direction were calculated:

$$P^o = \left(\frac{I}{I_o}\right)^{\frac{T}{M}}, \quad \tau = -\ln P^o \quad (1)$$

where I - direct radiation which passed through the cloud, I_o - direct radiation when the sun's disk is not occluded by clouds; M - cosec h_{\odot} ; h_{\odot} is the sun's height over the horizon.

I_o was determined either from measurements in breaks between clouds or from measurements on a day close to the cloudy day with a similar synoptic situation. On the basis of I_o values found this way, curves of its dependence on h_{\odot} were plotted, by means of which the value I_o was found for the same height of the sun as I.

Values of P^o and τ averaged over the types of cirrus clouds are listed in Table 4.1.

Table 4.1. High-level clouds' transmission coefficient (P^o) and optical thickness (τ) measured by an actinometer in 1986-1987.

Cloud Form	P^o					τ			
		Spectral region, nm				Spectral region, nm			
		$\lambda < 4000$	$\lambda < 525$	$\Delta \lambda = 380-710$	$\lambda > 710$	$\lambda < 4000$	$\lambda < 525$	$\Delta \lambda = 380-710$	$\lambda < 710$
Ci	med.	0.88	0.83	0.86	0.88	0.13	0.19	0.15	0.13
	n	106.00	49.00	77.00	85.00				
Cc	med.	0.90	0.81	0.88	0.86	0.11	0.21	0.13	0.15
	n	15.00	4.00	7.00	5.00				
Cs	med.	0.77	0.73	0.76	0.76	0.25	0.31	0.27	0.27
	n	11.00	7.00	11.00	11.00				
All forms	med.	0.87	0.82	0.85	0.86	0.14	0.20	0.16	0.15
	min.	0.55	0.50	0.56	0.53	0.01	0.02	0.01	0.01
	max.	0.99	0.98	0.99	0.99	0.59	0.69	0.58	0.64
	v%	11.00	15.00	12.00	12.00	80.00	76.00	76.00	81.00
	n	146.00	68.00	108.00	114.00				
All forms (data of simultaneous measurements)	med.	0.84	0.82	0.84	0.84	0.17	0.20	0.17	0.17
	v%	12.00	15.00	12.00	13.00	72.00	77.00	68.00	78.00
	n	66.00	66.00	66.00	66.00				

Note: n - number of cases; v - variation coefficient

Direct radiation is most strongly attenuated by cirrus-stratus (Cs) clouds. Transmission coefficients and the optical thicknesses of cirrus (Ci) and cirrus-cumulus (Cc) clouds are close to each other.

On average, the attenuation of I by cirrus clouds is not particularly spectrally dependent and is 12-14% for Ci, 10-14% for Cc, 23-24% for Cs and 13-15% for all forms of clouds. For the spectral region $\lambda < 525$ nm the attenuation is somewhat greater: 19-27%. However, perhaps the error of determining I in this spectral interval is larger than in other spectral intervals since I is determined from the small difference of large values.

It is evident from Table 4.1, that the number of measurements in different regions of the spectrum is not equal. To exclude the inhomogeneity of data due to a different number of cases average values of P^o and τ were determined from the data of simultaneous measurements in all spectral intervals. Despite the fact that for the spectral region $\lambda < 525$ nm the values of P^o were smaller, the differences proved to be statistically insignificant. This additionally buttresses the conclusion concerning the approximately neutral, on average, attenuation of direct radiation by high-level clouds.

It should be reminded (see Chapter 1) that values of τ obtained by the actinometer are cut by about 50% and that, correspondingly the real attenuation will be greater than that according to the data of Table 4.1. The same relates to histograms of the parameter τ represented in Figure 4.1.

4.2 Diffuse and global radiation

To evaluate the impact of cirrus clouds on Q and D , cases with a solid cloud cover were chosen. Global radiation according to the data of recording in the case of a solid high cloud cover was determined in one minute intervals and diffuse radiation in 30 minute intervals.

Table 4.2 lists mean (for all measurements), maximum and minimum values of global Q radiation in different regions of the spectrum.

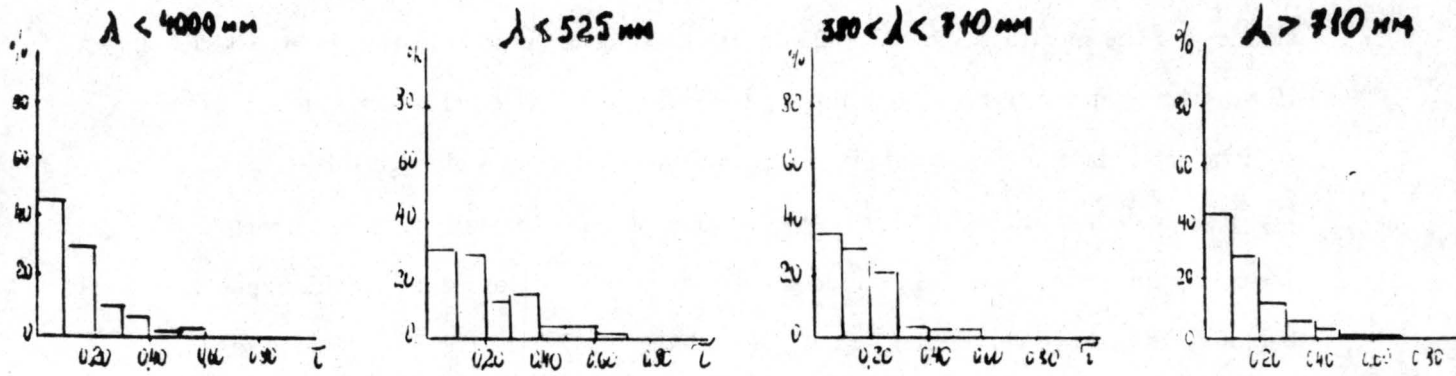


Figure 4.1: Recurrence of different values of the optical thickness of high clouds in different regions of the spectrum.

Table 4.2. Total solar radiation in different regions of the spectrum in conditions of the solid high cloud cover.

	Sun Height in Degrees								
Radiation	14.2	18.1	22.4	27.5	32.6	37.4	42.6	47.6	52.3
	Integral radiation, kw/sq m								
Mean	0.171	0.209	0.269	0.391	0.496	0.567	0.650	0.731	0.768
Maximum	0.192	0.262	0.355	0.484	0.613	0.730	0.804	0.843	0.873
Minimum	0.131	0.178	0.144	0.293	0.348	0.324	0.439	0.561	0.565
n	15	88	137	148	296	315	402	443	550
v%		11	19	12	14	15	12	10	9
	Ultraviolet radiation ($\lambda < 380$ nm), w/ sq m								
Mean	5.9	7.7	10.3	14.7	18.8	22.3	26.1	30.1	33.6
Maximum	6.3	9.2	12.8	17.0	23.8	26.5	32.2	34.2	38.8
Minimum	5.4	6.4	7.0	12.1	15.3	16.5	18.8	22.5	26.2
v%		10.0	14.0	10.0	16.0	11.0	12.0	10.0	7.0
	Photosynthetic active radiation ($\Delta\lambda = 380-710$ nm), kw/sq m								
Mean	0.072	0.093	0.121	0.183	0.227	0.264	0.307	0.349	0.380
Maximum	0.080	0.114	0.162	0.222	0.268	0.318	0.370	0.390	0.440
Minimum	0.060	0.080	0.060	0.144	0.176	0.170	0.224	0.268	0.288
v%		11.0	26.0	10.0	11.0	12.0	11.0	9.0	7.0
	Near infrared radiation ($\lambda > 710$ nm), kw/sq m								
Mean	0.093	0.108	0.138	0.193	0.250	0.281	0.317	0.352	0.354
Maximum	0.110	0.139	0.184	0.268	0.327	0.386	0.423	0.437	0.454
Minimum	0.066	0.086	0.067	0.137	0.154	0.138	0.188	0.247	0.239
v%		13.0	29.0	15.0	18.0	19.0	15.0	12.0	12.0

Note: n - number of cases; v - variation coefficient

Q in the sections of the spectrum discussed as a function of the sun's height for high clouds can be seen in Figure 4.2. The values of Q for the clear sky, when the transparency of the atmosphere was high ($\tau_{a,\lambda_0} = 0.10$) and low ($\tau_{a,\lambda_0} = 0.56$), are given here (τ_{a,λ_0} is the aerosol optical thickness of the atmosphere when $\lambda_0 = 0.55 \mu\text{m}$).

Regular variations of diffuse radiation can be traced from the ratio:

$$C_D = \frac{D}{D_0} \quad (2)$$

where D_0 - diffuse radiation when the sky is clear and there is aerosol turbidity close to that which was observed on days with cirrus clouds.

The results of calculations of C_D , given in Table 4.3, show an essential increase (with the exception of the UV region of the spectrum) of diffuse radiation in cirrus clouds which compensates to a large degree for the decrease of direct radiation. As a result, global radiation, as evident from Figure 4.2, varies only by a small amount.

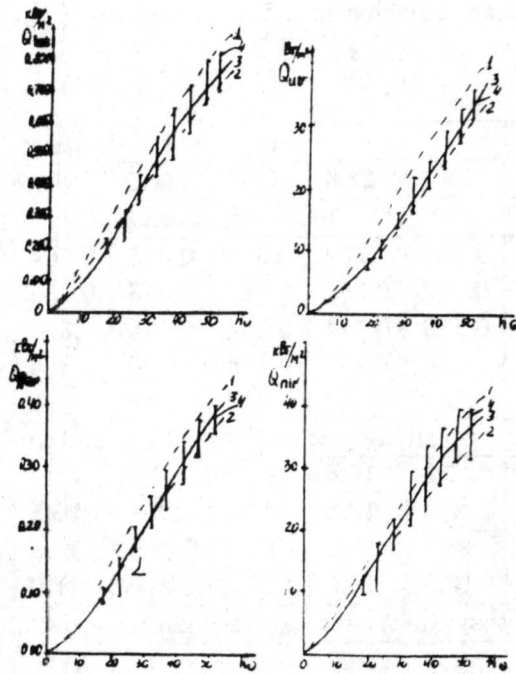


Figure 4.2: Global radiation in different regions of the spectrum as a function of the sun's height (h_{\odot}) in the cloudless sky (curves 1 and 2) and during a solid high cloud cover (curve 3 - mean data; vertical sections (4) - spread of measured values).

On average, high clouds attenuate (by 4-6% the global radiation in considered spectral regions.

On the basis of calculated values $C_Q = \frac{Q}{Q_0}$, histograms for different sections of the spectrum were plotted (Figure 4.3). The character of the distribution of C_Q for individual spectral intervals differs: the greatest C_Q range takes place in the case of near infrared radiation and the lowest in the case of ultraviolet radiation.

Let us note in conclusion that the effect of high clouds on the coming of diffuse and global radiation simultaneously in the ultraviolet, visible and near infrared sections of the spectrum and on the whole for entire solar radiation has been considered in detail for the first time.

On the whole, the results obtained are preliminary. To check and specify them, measurements for many years are needed.

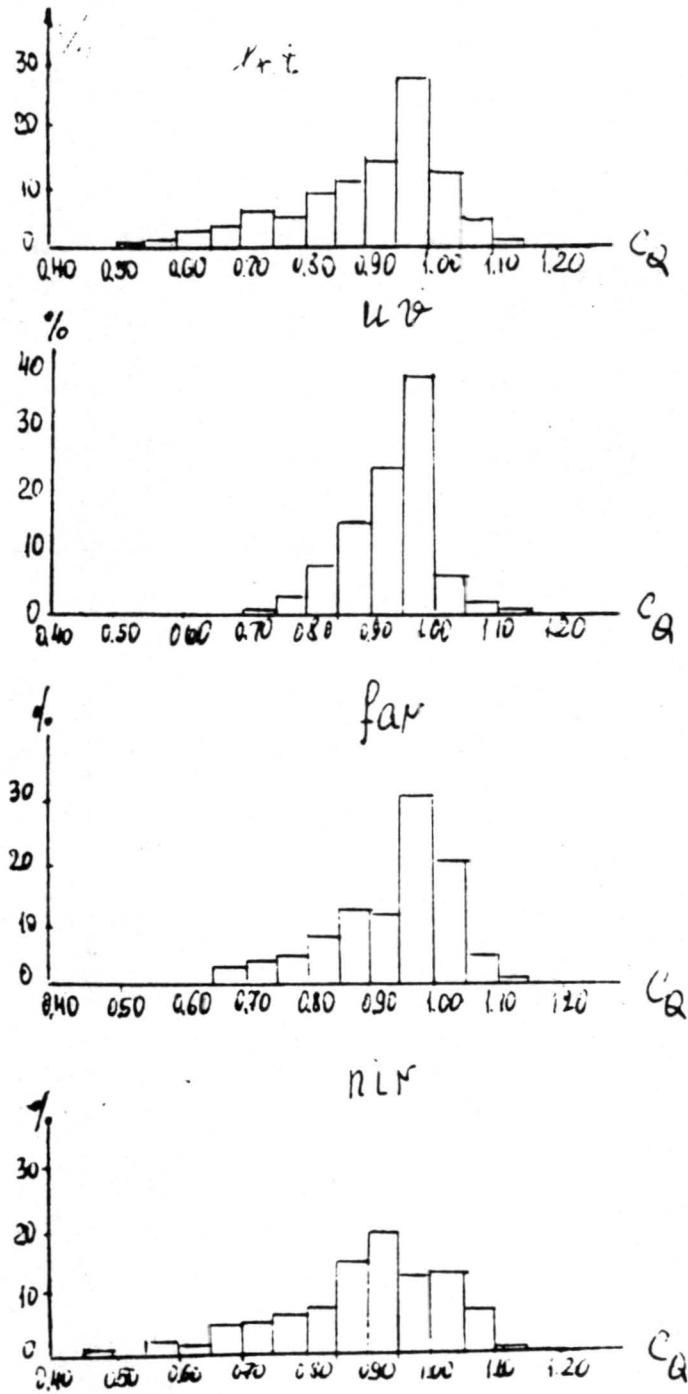


Figure 4.3: Recurrence of the global radiation transmission through a solid high cloud cover the ratio of the cloudless sky in different regions of the spectrum during the 1986-1987 experiment periods.

Table 4.3. The effect of high clouds on the ratio $C_D = \frac{D}{D_0}$

Spectral region	Mean	Maximum	Minimum	Number of cases	V%
INT	1.35	3.51	0.93	96	38
UV	0.97	1.17	0.75	117	8
PAR	1.14	1.89	0.81	113	17
NIR	1.62	3.65	1.01	110	34

Chapter 5

INTEGRAL THERMAL RADIATION FLUXES IN CIRRUS CLOUDS

In models of the general circulation of the atmosphere relating to the weather forecast and the climate theory, hemispherical fluxes integrated over the entire spectrum of infrared radiation (or over separate spectral intervals) are expressed to a certain approximation in the following form (see Feigelson, E. M., 1973).

$$F_{\uparrow}(Z) = B_S D(m) + \int_0^Z B(Z') dD[m(Z) - m(Z')] \quad (1)$$

$$F_{\downarrow}(Z) = - \int_Z^{\infty} B(Z') dD[m(Z') - m(Z)] \quad (2)$$

$D(m)$ is here an integral transmission function the argument of which is written conventionally. The basic absorbing gases in amounts $m_i(Z)$ in an atmospheric column $(0; Z)$ are meant here and in the case of clouds also their absorption by particles when there is the content $M_w(Z)$ in the column $(Z_b; Z)$. Here Z_b and Z_t are levels of lower and upper cloud boundaries.

Values B_S and $B(Z) \equiv B[T(Z)]$ are integrals with respect to λ from the Planck function at the temperatures of the surface and at the level Z .

In determining emissivity ϵ , fluxes on the boundaries of the cloud can naturally be represented in the form

$$F_{\uparrow}(Z_t) = \eta_{\uparrow} F_{\uparrow}(Z_b) + \epsilon_{\uparrow} B(Z_t) \quad (3)$$

$$F_{\downarrow}(Z_b) = \eta_{\downarrow} F_{\downarrow}(Z_t) + \epsilon_{\downarrow} B(Z_b) \quad (4)$$

Here $\eta_{\uparrow,\downarrow}$ are transmissions and if scattering is not taken into account, the conditions of equalities $\eta_{\uparrow,\downarrow} = 1 - \epsilon_{\uparrow,\downarrow}$ are satisfied.

Comparing (3) and (1) when $Z = Z_t$ and (4) with (2) when $Z = Z_b$, let us determine the integral values of $\eta_{\uparrow,\downarrow}$ and $\epsilon_{\uparrow,\downarrow}$. Let us also consider at first the flux $F_{\downarrow}(Z_b)$. We assume that the following conditions are satisfied.

Condition (a):

$$D(m' - m_t + \Delta m) = D(m' - m_t)D(\Delta m) \quad (5)$$

Here m' is the content of absorbing compound in the layer (O, Z') ;

$$m_t = m(Z_t); \Delta m = m_t - m_b; m_b = m(Z_b);$$

Condition (b):

$$B(Z) = \text{const when } Z_b \leq Z < Z_t$$

or

Condition (c):

$$\frac{dD[m(Z') - m_b]}{dZ'} \sim \delta[m(Z') - m_b] \quad (\delta - \text{delta function}),$$

i.e., the cloud is optically dense. From (2) it is easy to obtain

$$F_{\downarrow}(Z_b) = D(\Delta m)F_{\downarrow}(Z_t) + [1 - D(\Delta m)]B(Z_b) \quad (6)$$

i.e.,

$$\eta_{\downarrow} = D(\Delta m) \quad \text{and} \quad \epsilon_{\downarrow} = 1 - \eta_{\downarrow}$$

In a similar way, it is possible to obtain from (1) that

$$F_{\uparrow}(Z_t) = D(\Delta m)F_{\uparrow}(Z_b) + [1 - D(\Delta m)]B(Z_t) \quad (7)$$

while satisfying the conditions

$$D(m_b + \Delta m) = D(m_b)D(\Delta m) \quad (8)$$

and

$$D(m_t - m') = D(m_b - m')D(\Delta m) \quad \text{when } m' < m_b \quad (9)$$

as well as the condition (b) or

Condition (c):

$$\frac{dD[m_t - m(Z')]}{dZ'} \sim \delta[m_t - m(Z')]$$

We get: $\eta_{\uparrow} = \eta_{\downarrow}$ and $\epsilon_{\uparrow} = \epsilon_{\downarrow}$

Let us single out the ice component in the transmission function, assuming, as usual, that

$$D_{ice} = \exp[-Km_w^*], \quad (10)$$

irrespective of the wavelength. This, for example, is confirmed by calculations (Platt, C., and Stephens, G., 1980). In this case, if ratios (5), (8) and (9) are fulfilled, we have

$$\eta_{\uparrow} = \eta_{\downarrow} = D_g(\Delta m)\exp(-Km_w) \quad (11)$$

where D_g is the transmission function of the gas components in the cloud layer.

Ratios (5), (8) and (9) or the so-called multiplication principle is strictly fulfilled for the exponential function. The situation with the integral transmission function of the gas components or the transmission function in individual spectral intervals is quite different.

Ratio (8) for the integral transmission function was first checked in the paper (Zaitseva N. A., and Feigelson, E. M., 1979) for tropical cirrus clouds with the lower boundary level $Z_b = 7-13$ km and 2-5 km thick. It was obtained that

$$1.7 \leq \frac{D_g(m_b + \Delta m)}{D_g(m_b)D_g(\Delta m)} \leq 3$$

when

$$0.1 \leq \Delta m \leq 1.0 \text{ g/cm}^2,$$

$$m_b \approx 4 - 5 \text{ g/cm}^2.$$

Here and below m is a reduced (see: Feigelson, E. M., 1973) water vapor content according to data of measurements. The CO_2 content was assumed to be standard according to (McClatchey, R. *et al.*, 1972) and also recalculated as the reduced one. Hence, the ratio (8) is far from fulfilling as well as (5) and (9). Due to the Forbes effect, while moving to the cloud, the upward radiation traverses a large path, strong absorption lines are exhausted and $\frac{dD_g(m)}{dm}$ becomes small. Therefore, it is illogical to calculate m from the zero mass of gas components. According to the same data (Zaitseva, N. A., and Feigelson, E. M., 1979) in cases, when equation (5) is fulfilled with the error less than 10% when $m' = m^*$, we have evaluated the contribution of the gas component to transmission. In Table 5.1 the value η_1 is determined from eq. (4) on the basis of the measured fluxes and temperatures on cloud boundaries. The used values of $D_g(m^* - m_t)$ and $D_g(\Delta m)$ for gases H_2 and CO_2 are calculated in (Nijlisk, H. J., and Sammel, L. E., 1969) on the basis of (Davis, P., and Vieree, W., 1969). The table shows the essential contribution of gas absorption to transmission, and, correspondingly, to emissivity.

That's why we have not used equations (3 and 4) by $\epsilon = \epsilon_{ice}$, as it is usual, and corresponding (12 and 13) for the extra cloud atmosphere in calculations of integral thermal radiation fluxes.

$$F_{\uparrow}(Z) = F_{\uparrow}(Z_t)D_g[m(Z) - m(Z_t)] + \int_{Z_t}^Z B(Z')dD_g[m(Z) - m(Z')] \quad (12)$$

when $Z > Z_t$

$$F_{\downarrow}(Z) = F_{\downarrow}(Z_b)D_g[m_b - m(Z)] - \int_0^{Z_b} B(Z')dD_g[m(Z') - m(Z)] \quad (13)$$

when

$$Z < Z_b$$

Table 5.1. Some parameters of cirrus clouds in the tropics. Here m^* is the gas content in the thickness of the atmosphere.

N	$Z_b, (km)$	$Z_t, (km)$	$D_g(m^* - m_t)$	$D_g(\Delta m)$	$\eta \downarrow$	$\eta_{ice} = \frac{\eta \downarrow}{D_g(\Delta m)}$
1	12	16	0.90	0.85	0.47	0.55
2	9	14	0.90	0.63	0.51	0.81
3	12	15	0.92	0.86	0.75	0.87
4	12	16	0.95	0.86	0.57	0.60
5	13	15	0.92	0.90	0.83	0.93
6	13	16	0.96	0.89	0.67	0.76

We have applied a continuous approach recommended and used relating to water clouds by Feigelson, 1973. Use was made of equations 1 and 2 when $D(m)$ was of the following form:

For the flux $F_{\uparrow}(Z)$: (14)

$$D[m(Z)] = \begin{cases} D_g[m(Z)] & \text{if } Z < Z_b \\ D_g[m(Z)] \exp\{-K m_w(Z)\} & \text{if } Z \geq Z_b \end{cases}$$

For the flux $F_{\downarrow}(Z)$: (15)

$$D[m(Z)] = \begin{cases} D_g[m^* - m(Z)] & \text{if } Z < Z_t \\ D_g[m^* - m(Z)] \exp\{-K [m_w^*(Z) - m_w(Z)]\} & \text{if } Z \leq Z_t \end{cases}$$

The techniques, calculation results and assessments of errors are given in Feigelson, E. M., 1988; Gorchadova, I. A., and Feigelson, E. M., 1989; see also Collection "Radiative Properties of Cirrus Clouds," 1989).

The calculations are based on the data of the experiment. A few general remarks should be made.

1. Using the data of aerological sounding of the temperature $T(Z)$ and moisture $Q(Z)$ obtained over the distance of 80 km from the Zvenigorod Scientific Station, we

have leveled out profiles in such a way that $T(o)$ and $Q(o)$ coincided with those directly measured in the place of the experiment. The profile $Q(Z)$ was smoothed out according to the formula

$$Q(Z) = Q(o)e^{-Z/H}, \quad (16)$$

when H was determined from measurements of the total moisture content.

2. In the case of the continuous approach we must know the height distribution of ice inside the cloud $m_w(Z)$. We have supposed that $m_w(Z)$ is proportional to $\beta(Z)$ (see section II). In our case $km_w^* = \tau$ and, using data of section I, we assumed that the optical thickness of the cloud τ , irrespective of the wavelength, was equal to τ_λ when $\lambda = 10.2 \mu m$.

Referring to two cases of measurements conducted on May 11 and 24, 1986, let us consider the error of universally adopted equations (3 and 4) and (12 and 13) as compared with the continuous approach. At the same time, let us assess the effect of the different optical thickness of clouds on the fluxes. The results of calculations are presented in Table 5.2. Cloud boundaries were the following:

$$\text{May 11} \quad Z_b = 7.9 \text{ km} \quad Z_t = 8.2 \text{ km}$$

$$\text{May 24} \quad Z_b = 6 \text{ km} \quad Z_t = 8 \text{ km}$$

Table 5.2. Values of radiative fluxes coming from the cloud $F_{\uparrow}(Z_t)$ and $F_{\downarrow}(Z_b)$ and fluxes on the boundaries of the atmosphere $F_{\uparrow}(\infty)$ and $F_{\downarrow}(0)$ on May 11 and May 24, 1986. Column (1) - cloudless sky, column (2) - continuous approach, (3) - calculation according to formulas (3 and 4) and (12 and 13).

Fluxes $w/sq\ m$	May 11 $\tau = 0.18$			$\tau = 0.21$			May 24 $\tau = 0.53$		$\tau = 1.2$	
	(1)	(2)	(3)	(1)	(2)	(3)	(2)	(3)	(2)	(3)
$F_{\uparrow}(Z_t)$	248	232	210	277	255	228	233	212	211	197
$F_{\uparrow}(\infty)$	220	205	166	235	216	176	196	169	176	163
$F_{\downarrow}(0)$	236	245	273	307	321	349	335	353	350	358
$F_{\downarrow}(Z_b)$	70.3	86.0	104	132	158	191	184	210	211	229

Let us consider the error of calculating clouds' own radiation, i.e., the second components in (3 and 4) while using these formulae. Apparently the error is small for thin cloud layers. In the case of thick layers $B(Z_t)$ must be replaced by B_1 while $B(Z_b)$ by B_2 expressed by ratios:

$$B_1 = \frac{\int_{Z_b}^{Z_t} B(Z') dD[m_t - m']}{1 - D[m_t - m_b]}$$

$$B_2 = \frac{\int_{Z_b}^{Z_t} B(Z') dD[m' - m_b]}{1 - D[m_t - m_b]} \quad (17)$$

In Table 5.3 for May 24, 1986, values B_1 and B_2 are given depending on the position of max $W(Z)$

$$\text{where } W(Z) = \frac{dM_w(Z)}{dZ}$$

Table 5.3. Values B_1 and B_2

1. max $W(Z)$ - near the upper boundary;
2. in the center of the cloud;
3. near the lower boundary.

B_1 w/sq m			$B(Z_t)$ w/sq m	B_2 w/sq m			$B(Z_b)$ w/sq m
(1)	(2)	(3)		(1)	(2)	(3)	
193	200	222	190	214	222	235	238

Thus, the error of formulae (3 and 4) can be great, if the thick cloud's own radiation is referred to its boundaries.

Let us assess the error of equations (3 and 4) due to the disregard of gas absorption. Assuming that fluxes calculated by the continuous method are exact (at least their error is the same as in the cloudless case), let us substitute their values into (3 and 4). Let us determine η and $D_g(\Delta m) = \frac{\eta}{e^{-1.66\tau}}$.

The values of D_g obtained are listed in Table 5.4.

Table 5.4. True values of D_g ; May 24, 1986.

τ	$D_{g,\uparrow}(\Delta m)$	$D_{g,\downarrow}(\Delta m)$
0.21	0.72	0.71
0.53	0.73	0.70
1.2	0.76	0.76

We see that the true values of $D_g(\Delta m)$ are far enough from unity. However, it is not clear how an a priori method of determining these true values can be evolved, as well as $D_g[m(Z) - m_t]$, $D_g[m_b - m(Z)]$ in eqs. (12 and 13).

Therefore, we recommend that the continuous approach should be used for calculating integral thermal radiation fluxes. The advantage of this method is obvious: a single algorithm of calculations for cases when the sky is cloudy and when it is clear. Fluxes and influxes of thermal radiation on May 11 and 24, 1986 and on May 19, 20 and 22, 1987 were calculated to this approximation.

The values of fluxes as compared with the case of the clear sky are given in Table 5.2 for 1986 and in Table 5.5, 1987. Table 5.6 gives the radiative cooling of the atmospheric thickness, the above-cloud, subcloud and cloud layers. This table shows that as compared with the case of the clear sky the atmosphere becomes warmer during the cloudy sky. The same is true of the subcloud layer. The above-cloud layer is cooling. The cloud, depending on its height, thickness and temperature and moisture distribution, can become warmer or colder than the corresponding layer of the cloudless atmosphere.

Let us discuss in conclusion the problem of taking into account the reflection of the flux $F_{\uparrow}(Z_b)$ by the cloud within the framework of the same parameterization. For the sake of simplicity we can limit ourselves to the slight increase of the coefficient k in eq. (10). However, the possibility of taking into account actual variations of $F_{\uparrow}(Z_b)$ is then lost. The second possibility is to calculate the flux $F_{\downarrow}(Z_t)$ from eq. (4) to which the component $AF_{\uparrow}(Z_b)$ is added.

The albedo A can be determined, for instance, in the dependence on m_w^* according to the data of the paper (Liou, K. N., and Wittman, G. D., 1979) which represent, however, a particular case: $Z_b = 4.6$, particles are cylindrical when $\ell = 200 \mu m$, $r = 30 \mu m$, and the number of particles is $0.05 cm^{-3}$. In (Feigelson, E. M., 1988) a more general, although approximate approach has been presented. The formula obtained makes it possible to change the flux $F_{\uparrow}(Z_b)$ and also the optical parameters of the cloud:

$$F_{\downarrow}(Z_b) = \epsilon \frac{\omega F_{\uparrow}(Z_b) \Gamma_2 + (1 - \omega) B(Z_b)}{1 - \omega \Gamma_1 \epsilon} \quad (18)$$

where $\Gamma_1 = \int_0^1 \gamma(\psi) d\cos\psi$, $\Gamma_2 = \int_1^0 \gamma(\psi) d\cos\psi$, $\gamma(\psi)$ is the scattering function, ψ is the scattering angle, and ω is the single scattering albedo.

Table 5.5. Integral heat radiation fluxes for the year 1987.

Date	May 19		May 20		May 22	
Fluxes $W m^{-2}$	clear sky $\tau = 0.33$	cloudy sky	clear sky $\tau = 0.17$	cloudy sky	clear sky $\tau = 0.46$	cloudy sky
$F_{\uparrow}(Z_t)$	240	206	241	218	254	217
$F_{\uparrow}(\infty)$	216	186	223	203	208	179
$F_{\downarrow}(Z_b)$	93	124	95	111	117	156
$F_{\downarrow}(0)$	309	321	344	350	372	383

Table 5.6. Positive sign is radiative cooling for separate layers. Minus signifies heating for cloudy layers. The year is 1987.

Date	May 19		May 20		May 22	
Layers	clear sky $\tau = 0.33$	cloudy sky	clear sky $\tau = 0.17$	cloudy sky	clear sky $\tau = 0.46$	cloudy sky
Entire atmospheric thickness	121	104	123	110	131	113
Subcloud Layer	68	49	70	60	71	43
Cloud Layer	1.9	-1.9	1.8	-4.7	2.3	4.2
Above Cloud Layer	52	56	51	54	58	66

Chapter 6

OPTICAL MODELS, CALCULATION OF SOLAR RADIATION FLUXES AND RADIATION BALANCE

6.1 Optical Properties of Crystals

As shown in Pruppacher and Klett, (1978), ice crystals in cirrus clouds vary in size ranging from several micrometers to several millimeters. Crystals can orient themselves in space, but their orientation during free fall in the atmosphere is studied insufficiently. Therefore, this orientation is most frequently assumed to be chaotic. Crystals are usually shaped as hexagonal prisms, spheroids or circular cylinders. Methods of determining the optical characteristics of an elementary volume required for calculating solar radiative transfer have been developed. The asymmetry factor of phase function $P(\theta)$ is

$$g = \int_{4\pi} \frac{P(\theta)}{4\pi} \cos \theta d\omega$$

where θ is the angle of scattering; ϵ is the attenuation coefficient; $\omega = \frac{\delta}{\epsilon}$ is the single scattering albedo where δ is the scattering coefficient.

In papers by Welch, *et al.* (1980); and Plass and Kattawar, (1971) these parameters are calculated for large spherical particles with the gamma distribution of the number of particles in size and with modal radii $20 < a_m < 600 \mu m$.

In Liou, (1973) these parameters are calculated for individual monodisperse cylinders with the ratio of the length to the diameter (shape factor) $c = \ell/d = 200/60 \mu m$ for several wavelengths of the solar spectrum. Phase function calculated in Wendling *et al.*, (1979); and Liou, (1986) for hexagonal prisms $300/60 \mu m$ have a sharply pronounced

halo which leads to doubtfully large values of $g = 0.99$ when $\lambda = 0.55 \mu\text{m}$. No studies were made of the optical characteristics of nonspherical particles as a function of the size and the shape factor in the case of the polydisperse distribution of the number of crystals in lengths which is usually observed in clouds (Heymsfield, 1975a). No detailed spectral dependencies of optical parameters in the entire range of the solar spectrum were obtained. The possibilities of using the model of equivalent spheres were analyzed only for attenuation coefficients. In Volkovitsky *et al.*, (1984) the technique of determining ϵ , g and ω for hexagonal prisms with the gamma-distribution of particles in size was described and some calculations were made. In our paper, using the above technique, more detailed calculations were conducted for hexagonal ice prisms large as compared with the wavelength and having chaotic orientation in space. As a distribution of these particles the lengths ℓ a gamma distribution was used.

$$f(\ell)d\ell = A\ell^\mu \exp(-\mu\ell/\ell_m)d\ell \quad (1)$$

where A is the normalization constant, ℓ_m is the modal length of the prism, μ is the gamma-distribution parameter assumed by us as $\mu = 6$. We considered the fraction of large ice particles with $50 < \ell_m < 10^3 \mu\text{m}$, the shape factor varied within $0.5 < C < 6$, and the refractive index of the material of ice m was taken from Irvine and Pollack, (1978).

6.2 The Radiation Phase Function and the Assymetry Factor of the Phase Function

Phase functions of large ice prisms were calculated to an approximation of geometrical optics with due account for diffraction (Volkovitsky *et al.*, 1984). A typical phase function for sizes indicated in the figure caption is given in Figure 6.1. When $\theta > \theta_d(0 - \theta_d$ - range of small scattering angles in which diffraction prevails) with the exception of the halo's ranges $\theta \sim 22$ degrees and $\theta \sim 46$ degrees and backscattering $\theta \sim 180$ degrees the phase function mainly depends on the shape factor of particles and the magnitude of the

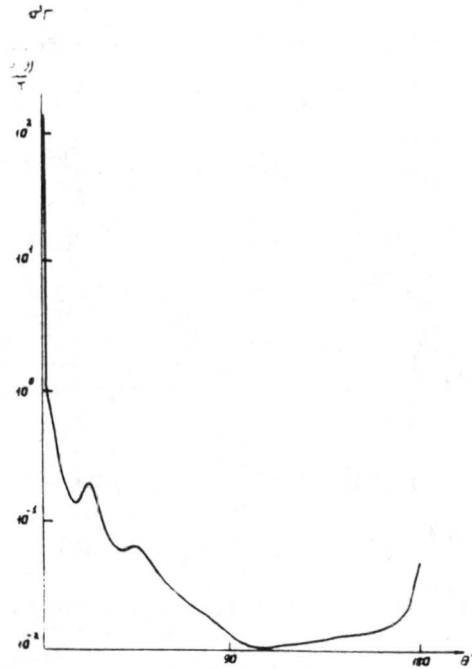


Figure 6.1: Phase function of visible radiation $\lambda = 0.63 \mu m$ by a system of hexagonal prisms with gamma-distribution in lengths ($l_m = 200$, $C = 4$).

complex refractive index $m = n - ix$. When $\theta < \theta_d$, the scattering essentially depends on the size of hexagonal prisms. When $\theta = 0$, the magnitude of ratio $\frac{P(\theta)|_{pr}}{P(\theta)|_{sph}} > 1$, irrespective of the shape factor of prisms. With an increase of the scattering angle this ratio becomes greater than unity to a larger extent in the case of large dimensions of scattering particles. However, let us note that in the considered range of sizes $20 \mu m < l_m < 400 \mu m$, $0.5 < C < 6$ and with $\theta < 4^\circ$ the difference of the values of phase function for prisms and model ice spheres is lower than 30%. Thus, the model of spherical particles having the same area of the surface as hexagonal prisms describes with the satisfactory accuracy the scattering by a system of hexagonal prisms for small angles $\theta < \theta_d$. When $\theta > \theta_d$ no models of spherical particles represent scattering on prisms since the specific features of such scattering are mainly determined by particles' nonspherical shape.

Table 6.1 lists data on the assymetry factor calculated for different models of the microstructure of the crystalline medium by some authors and obtained experimentally. In the general case, nonsphericity leads to the decrease of g , excluding data from Liou,

(1986). Values of g were determined by us through the numerical integration of the phase function obtained. Since for particles with sizes considerably exceeding the wavelength of incident radiation the emission flux is scattered with θ from 0 to θ_d is roughly equal to the scattered flux with θ from θ_d to π , the expression for g can be written in the form:

$$g = \frac{1}{2} \left\{ \frac{\int_0^{\theta_d} \frac{P(\theta)}{4\pi} \cos \theta \sin \theta d\theta}{\int_0^{\theta_d} \frac{P(\theta)}{4\pi} \sin \theta d\theta} + \frac{\int_{\theta_d}^{\pi} \frac{P(\theta)}{4\pi} \cos \theta \sin \theta d\theta}{\int_{\theta_d}^{\pi} \frac{P(\theta)}{4\pi} \sin \theta d\theta} \right\}. \quad (2)$$

With the increase of the size of prisms the first component slightly increases in size, tending to its limit value of 0.5. The second component practically does not depend on dimensions. Thus, the assymetry factor with the increase of the size of prisms with the fixed shape of the latter tends to a certain limit value. It is worth noting that the limit values of assymetry factors were detected earlier for large spherical particles Van de Hulst, (1957), and that these limit values are only a function of the complex refractive index for wavelengths under consideration. For large spherical particles, when $\lambda = 0.6 \mu m$ in Van de Hulst, (1957), $g = 0.87$ was obtained irrespective of dimensions. The result of the integration of the phase function by hexagonal prisms represented in Figure 6.1 is the value $g = 0.74$. The main contribution to the shaping of g is made by the angle range of 10 to 50 degrees the scattering in which is determined mainly by the shape factor (in this case $C = 4$) and by the refractive index of ice.

Table 6.1

The Assymetry Factor of the Phase Function						
Shape	Size	Wavelength	g	Note	Source	
1	2	3	4	5	6	
spheres	$a_m=5$	0.55-1.8	0.86	a_m - modal radius of the gamma-distribution. Use is made of the value $m=n-i\epsilon$ which is average for wavelength interval a - radius of the sphere	Welch <i>et al.</i> , 1980	
		1.80-2.8	0.95			
	$a_m=20$	0.55-1.8	0.89			
		2.80-3.3	0.97			
	$a_m=70$	0.55-1.8	0.87-0.94			
		2.80-3.3	0.99-0.96			
$a_m=330$	0.55-1.8	0.84-0.93				
	2.80-3.3	0.98-0.95				
	$a_m=600$	0.55-1.8	0.88-0.94		Plass, Kattawar, 1971	
		2.80-3.3	0.97-0.94			
		0.7	0.79			
		1.7	0.84			
		2.1	0.86			
		2.96	0.98			
cylinders	$a_m=200$	0.7	0.735	ℓ - length of cylinder d - diameter	Liou, 1973	
		2.0	0.750			
		$a_m=60$	2.5			0.753
		3.0	0.651			
hexagonal	$\ell=300$ $d=60$	0.55	0.988		Liou, 1986	
		0.7	0.987			
		1.3	0.985			
		3.8	0.982			
		10.6	0.975			
spheroids	$8 < a < 24$	11	0.8-0.97	a - major axis B - minor axis $3 \leq a/B \leq 5$	Asano,	
non-spherical	5-200	0.55	0.73	Indicatrix is obtained experimentally	Pavlova <i>et al.</i> , 1981	
-"	$d \approx 10$	10.05	0.83	-"	Sassen, 1981	
hexagonal prisms	$50 < \ell_m < 250$ $40 < \ell_m < 200$	0.63 1.7	$g_I \approx 0.74$ $g_I \approx 0.84$ $g_I \approx 0.87$	Arbitrary orientation prisms' axes in the horizontal plane. I - orientation plane, II - plane perpendicular to to plane I and passing through the direction of incident radiation	Volkovitsky <i>et al.</i> , 1984	

6.3 Albedo of Single Scattering

In this work we discuss the results of our calculations of the albedo of single scattering (ω) both by individual hexagonal prisms and by systems of hexagonal prisms in the case

of arbitrary values of shape factors C and the chaotic orientation in space. The sizes of crystals varied within the range $10^2 < \ell_m < 10^4 \mu m$, values $0.5 < C < 6$. The used calculation procedure to the approximation of geometric optics made it possible to take into account the contribution to absorption by multiple acts of refraction and reflection on lateral facets of the prism, as well as single reflection and refraction on butt-ends of the prism.

The results of calculations we have carried out show that when $\lambda \leq 1.2 \mu m$ in the considered range of values of ℓ_m , the value ω can essentially differ from 1 only when $\ell_m > 10^3 \mu m$. With the increase of λ the value ω greatly depends on the size and can assume the value ranging from 0.6 to 0.9. As an effective size of hexagonal prisms in describing the single scattering albedo let us use the ratio of the volume of crystals to the area of the geometrical shadow. This effective size was first proposed in (Van de Hulst, 1957) for describing the attenuation by systems of spherical particles.

The comparison of the calculations of ω for systems of hexagonal prisms, circular cylinders of the finite length (Liou, 1973) with calculations for large ice spheres with effective radii carried out according to the Mie theory shows satisfactory agreement. In the range of wavelengths of incident radiation $\lambda = 0.63 - 2.5 \mu m$ it is rational to use approximate expressions for ω of ice particles

$$\omega = \begin{cases} 1 - 0.5f(n)\gamma a_{xp} & \gamma a_{xp} < 0.1 \\ 0.5 + 0.5 \exp(f^k(n)\gamma a_{xp}) & k = 1 \quad \gamma a_{xp} < 0.5 \\ & k = 2 \quad 0.5 < \gamma a_{xp} < 2.5 \\ 0.5 + 0.5 \omega_0 & \gamma a_{xp} > 5 \end{cases} \quad (3)$$

for individual particles,

$$\omega = 0.5 + 0.5 \left[1 + \frac{f^2(n)a_{xp}\gamma}{(\mu + 3)} \right]^{-(\mu+3)} \quad (4)$$

for systems of particles with gamma-distribution with respect to size where μ is the gamma-distribution parameter, a_{zp} is

$$a_{zp} = 4\ell_o(1 + \frac{8}{\sqrt{3}}C)^{-1} \quad (5)$$

ℓ_o is the length of the prism ℓ for individual particles, modal length ℓ_m for systems of particles, $f(n)$ is

$$f(n) = n^2(1 - (\frac{n^2 - 1}{n^2})^{\frac{3}{2}}), \gamma = \frac{4\pi}{\lambda} \quad (6)$$

and ω_o is the share of radiation reflected by a sphere (Kerker, 1969).

The application of these expressions for the calculation of ω by hexagonal prisms leads to the absolute error not higher than 0.05 in the entire range of considered dimensions of prisms. In the case of using calculations for spherical particles with effective radii according to the Mie theory for describing ω by ice crystals the absolute error will be lower than that mentioned above.

6.4 Calculation of Fluxes Based on Experimental Data

Table 6.2 gives four models of the optical characteristics of the cloud layer which are used in calculations. The increase of g with the considerable absorption of ice by substance was ignored when $\lambda > 2.5 \mu m$ due to the weak influence of g on radiative transfer in this case. The values of ω_2 ($.3 < \lambda < 1.2 \mu m$) equal to 0.6 (models II and IV) were assumed as the possible limit for very large particles. Spectral optical thickness of clouds (τ_λ) were determined from measurements of solar radiation passed through a radiometer. Since the sizes of crystals were much larger than the wavelength, a neutral variation of the attenuation coefficient with respect to the spectrum was assumed. We used average values of $\bar{\tau}$ for 0.5 hr when $\lambda = 10 \mu m$, which were free from the multiple scattering effect.

Table 6.2. Optical characteristics of particles of different shapes. The value of g corresponds to the spectral interval $0.3 < \lambda < 4 \mu\text{m}$. $\omega_1)0.3 < \lambda < 1.2 \mu\text{m}$, $\omega_2)1.2 < \lambda < 2.5 \mu\text{m}$, $\omega_3)\lambda > 2.5 \mu\text{m}$.

Model Shape	$C = \frac{t}{2a}$	g	ω		
			ω_1	ω_2	ω_3
I spherical	1	0.9	1	0.9	0.5
II			1	0.6	0.5
III hexagonal prisms	4	0.7	1	0.9	0.5
IV			1	0.6	0.5

The optical characteristics of the extra cloud atmosphere were determined in the course of the experiment or varied within wide limits in accordance with various aerosol models. The results are given in Table 6.3. It was assumed that the aerosol optical thickness τ_{a,λ_0} and the mass of water vapor m_ν varied slightly in the daytime. The value τ_{a,λ_0} was determined from measurements of direct solar radiation ($0.38 < \lambda < 0.71 \mu\text{m}$) according to the technique of Abakumova *et al.*, 1989, and the value m_ν from aerosol soundings.

To calculate the integral fluxes of solar radiation use was made of a three-layer model of the cloud-aerosol atmosphere. In the lower layer we took into account molecular scattering, absorption and scattering by aerosol, absorption by water vapor, in the middle layer, scattering and absorption by ice crystals, and in the upper layer molecular scattering and absorption by aerosol. Calculations were carried out by Eddington's two-flux method (Joseph *et al.*, 1976) in 12 spectral intervals from $\lambda = 0.3 \mu\text{m}$ to $\lambda = 4 \mu\text{m}$ including water vapor bands and intervals between them. In water vapor bands, use was made of the expansion of the function of water vapor transmission into a series with respect to five exponents, which is presented in Liou and Sasamory, (1975). We calculated integral ($0.3 < \lambda < 4 \mu\text{m}$) and in the photosynthetically active radiation ($0.38 < 0.71 \mu\text{m}$) range, global radiation near the surface Q . The system's albedo was also calculated. The atmo-

sphere is an underlying surface within the same range. The spectrum of the solar constant from (WCP-149, 1986) was used.

The albedo of the surface was given within the limits $\tau_s = 0.1 - 0.2$ which corresponds to the albedo of grass and coniferous forests (Kondratyev, 1960).

To compare calculated (Q_{calc}) and measured (Q_{meas}) fluxes we chose 1986 and 1987 observation periods which are characterized by almost solid cirrus clouds (cloudiness class $n = 8...10$) with the absence of other forms of clouds in the sky. The range of changes of clouds' optical thickness was $\tau = 0.2 - 1.2$.

The results of measurements and calculations are summarized up in Table 6.4-6.6. The interval of values Q_{calc} and r corresponds to those indicated in the table and to ranges of the change of optical parameters. Values of Q_{calc} and Q_{meas} agree within the limits of the error of calculations and measurements which is on the order of 10%.

Table 6.3. The water vapor mass in the vertical column of the atmosphere - m_v , aerosol optical parameters - τ_{a,λ_0} ; g_{a,λ_0} ; ω_{a,λ_0} ; and their spectral variations in the above-cloud layer and the subcloud layer; n is the exponent in the formula $\tau_{a,\lambda} = \tau_{a,\lambda_0}(\frac{\lambda_0}{\lambda})^n$. Aerosol models used: 1) "rural", 2) "background stratospheric" WCP-55, 1983).

	τ_{a,λ_0}	m_v	g_{a,λ_0}		ω_{a,λ_0}
subcloud	See Table 6.2	See Table 6.2	0.55 - 0.65 (Tarasova, Feigelson, 1981)	0.9 - 0.99 0.93 from 1)	(Tarasova, Feigelson, 1981)
above- cloud	0.02	-	0.7	0.7	0.99

Spectral Dependencies			
	$\tau_{a,\lambda}$	$g_{a,\lambda}$	$\omega_{a,\lambda}$
subcloud	$n = 1-2$ and from 1)	$g_{a,\lambda} = g_{a,\lambda_0}$ and from 1)	$\omega_{a,\lambda} = \omega_{a,\lambda_0}$ and from 1)
above- cloud	from 2)	from 2)	from 2)

Table 6.4. Calculated and measured integral fluxes of global radiation near the surface Q with the Ci (cl) and clear (clear) sky for 1986. The table lists ratios C_Q characterizing variations of the flux passed through clouds and C_r - variations of the reflected flux.

	11.V.86			24.V.86		
Moscow time	14-15	12-12.30	15.30-16	12.30-13	13.0-13.30	14-15.30
$\mu_o = \cos Q_o$	0.771	0.79	0.729	0.807	0.817	0.763
$\bar{\tau}$	0.18	0.17	0.41	0.41	0.75	1.2
τ_{a,λ_o}	0.15-0.25	0.3-0.5	0.3-0.5	0.3-0.5	0.3-0.5	0.3-0.5
$m_\nu, g/cm^2$	0.5	1.8	1.8	1.8	1.8	1.8
Q_{cl}^{calc}	850-784	823-718	745-611	831-701	827-666	738-554
Q_{cl}^{meas}	862	816	719	805	765	660
Q_{clear}^{meas}	860-799	837-745	762-673	858-765	870-777	804-713
Q_{clear}^{meas}	839	797	723	817	827	767
C_Q^{calc}	0.99-0.98	0.98-0.96	0.96-0.91	0.97-0.92	0.95-0.86	0.91-0.78
C_Q^{meas}	1.02	1.02	1.00	0.99	0.94	0.86
C_r^{calc}	1.12-1.01	1.09-1.00	1.23-1.02	1.23-1.01	1.38-1.03	1.6-1.07

Table 6.5. The same as in Table 6.1, but for fluxes in the region of wavelengths of photosynthetically active radiation ($0.38 \leq \lambda \leq 0.71 \mu m$).

	11.V.86			24.V.86		
Moscow time	14.00-15.00	12.00-12.30	15.30-16.00	12.30-13.00	13.00-13.30	15.00-15.30
μ_o	0.771	0.79	0.729	0.807	0.817	0.763
Q_{cl}^{calc}	399-365	401-346	361-300	408-343	409-333	368-285
Q_{cl}^{meas}	381	412	364	408	399	344
Q_{clear}^{calc}	402-375	403-354	367-320	414-364	420-370	388-339
Q_{clear}^{meas}	387	397	359	408	415	381
C_Q^{calc}	0.99-0.97	1.00-0.98	0.98-0.94	0.99-0.94	0.97-0.9	0.95-0.84
C_Q^{meas}	0.99	1.04	1.01	1.00	0.95	0.94
C_r^{calc}	1.09-1.02	1.06-1.02	1.17-1.05	1.17-1.04	1.29-1.08	1.45-1.13

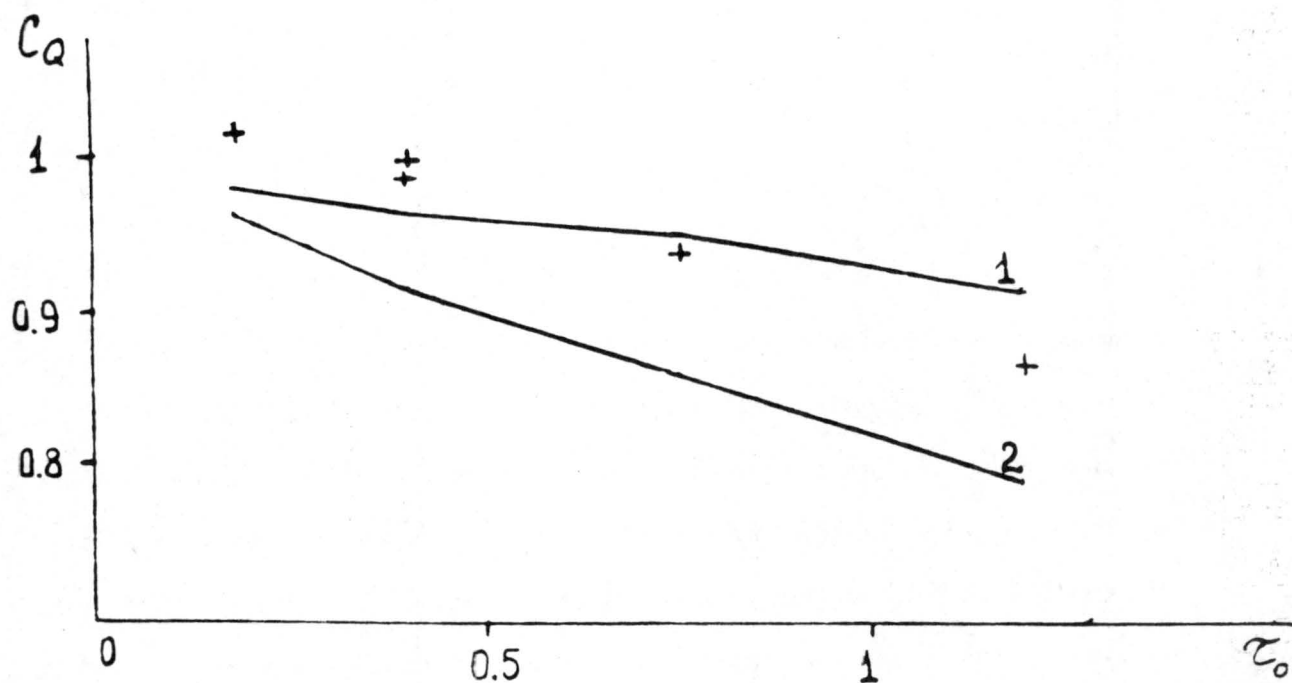


Figure 6.2: C_Q value for observation periods indicated in Tables 6.1 and 6.3. This value is calculated for two models giving the minimum and maximum values: I and IV.

Table 6.6. The same as in Tables 6.1 and 6.2, but for 1987

	Integral Radiation				Photosynthetically Active Radiation			
	19.V.87	17.30-18	20.V.87	22.V.87	19.V.87	20.V.87	22.V.87	
Moscow time	14-14.30	17.30-18	11.30-12	13.30-14	14-14.30	17.30-18	11.30-12	13.30-14
$\mu_0 = \cos\theta_0$	0.80	0.51	0.76	0.81	0.80	0.51	0.76	0.81
$\bar{\tau}$	0.32	0.33	0.17	0.46	0.32	0.33	0.17	0.46
τ_a, λ_0	0.2-0.3	0.2-0.3	0.45-0.60	0.45-0.60	0.2-0.3	0.2-0.3	0.45-0.60	0.45-0.60
$m_\nu, g/cm^2$	1.3	1.3	1.9	2.8	1.3	1.3	1.9	2.8
Q_{cl}^{calc}	845-756	494-420	758-655	807-672	409-367	239-205	372-314	402-332
Q_{cl}^{meas}	750	391	719	721	366	189	350	358
Q_{clear}^{calc}	862-809	513-469	767-681	829-741	414-383	245-220	374-323	409-355
Q_{clear}^{meas}	850	475	779	865	421	224	380	425
C_Q^{calc}	0.98-0.93	0.96-0.9	0.99-0.96	0.97-0.91	0.99-0.96	0.98-0.93	0.99-0.97	0.98-0.94
C_Q^{meas}	0.88	0.82	0.92	0.83	0.87	0.84	0.92	0.84
C_Q^{calc}	1.21-1.00	1.27-1.04	1.10-1.00	1.23-1.02	1.15-1.03	1.19-1.06	1.06-1.02	1.16-1.04

To assess quantitatively the effect of C_i on the global radiation flux we have calculated the ratio of fluxes during cloudiness and when the sky is clear. This ratio is given in Tables 6.4-6.6 and in Figure 6.2.

The values C_Q are determined by the optical parameters of the cloud τ, g, ω_2 . The linear approximation

$$C_Q = 1 - 0.19\tau'$$

$$\tau' = (1 - g^2\omega_2) \frac{\tau}{\mu_0} \quad (7)$$

is carried out with good accuracy. The error of calculating C_Q by the formula is less than 1% when $\tau < 1$ and less than 2% when $\tau > 1$. It is evident from Tables 6.4-6.6 that calculated values of C_Q are in good agreement with measured values, with the exception of thin clouds $0.1 < \tau < 0.2$ when $C_Q^{meas} > 1$. In all probability this effect is due to the greatly broken field of thin cirrus clouds. In this case the contribution of direct solar radiation to global radiation can be greater than in the model of a homogeneous cloud layer used in calculations.

The influence of the microstructure of the cloud and albedo of the underlying surface (α_s) on the change of the albedo system by the cloud $C_r = A_{cl}/A_{clear}$ is presented in Figure 6.3 for two extreme cases (models II and III). Relying on the approximation of calculations for changing the albedo of the atmosphere by the cloud $C_{r_a} = \frac{r_a^{cl}}{r_a^{cloud}} = 1 + K(g)\tau$ where $k = 0.4$ when $g = 0.9$ and $k = 0.8$ when $g = 0.7$, it is possible to obtain a simple approximated formula for determining C_r from the value C_Q .

$$C_r = \frac{1 + k(g)\tau}{1 + r_s/0.14} + \frac{r_s C_Q^2}{r_s + 0.14} \quad (8)$$

The error of eq. (8) is less than 3% when $\tau < 1$ and less than 5% when $\tau > 1$.

6.5 Radiation Balance for Solar and Thermal Radiation

The radiation balance of the upper boundary of the atmosphere $F(\infty)$ in the presence of cirrus clouds and for the cloudless atmosphere was obtained from the formula

$$F(\infty) = I_0\mu_0(1 - r) - F_{\uparrow} \quad (9)$$

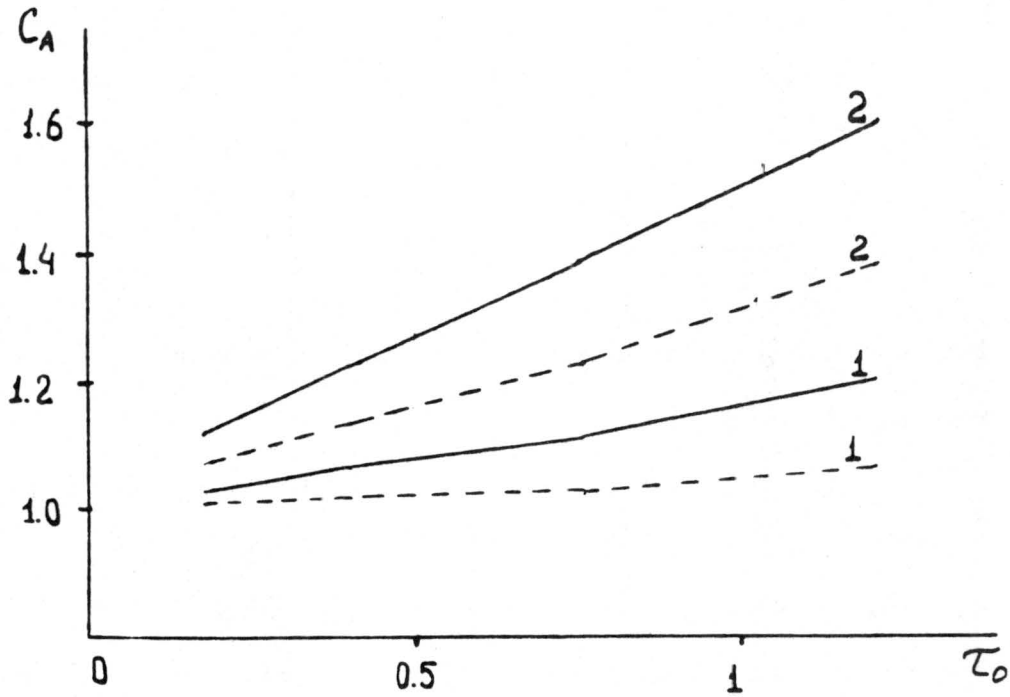


Figure 6.3: Value C_A with different albedos of the surface (solid curves - $A_S = 0.1$, dashed curves - $A_S = 0.2$) for two models giving the maximum and minimum values: II and III.

where I_o - solar constant, μ_o - cosine of the sun's zenith angle. F_{\uparrow} outgoing thermal radiation flux calculated from the data of the experiment. High clouds reduce F_{\uparrow} , heating the system and increase r cooling it. Depending on the ratio of these opposite trends the value of the change of the radiation balanced by the cloud $\Delta F(\infty) = F_{cl}(\infty) - F_{clear}(\infty)$ can have a different sign: a positive sign when clouds raise the temperature and a negative sign in the opposite case.

We have also calculated the variation of the radiation balance of the underlying surface in the cloudy sky as compared with the cloudless atmosphere

$$\Delta F(0) = F_{cl}(0) - F_{clear}(0) \quad (10)$$

where $F(0) = F_{\downarrow}(0) - F_{\uparrow}(0) + I_o \mu_o t (1 - r)$

- $F_{\uparrow}(0)$ - thermal radiation of the surface
- $F_{\downarrow}(0)$ - counter-radiation of the atmosphere,
- t - transmission of the atmosphere for solar radiation.

We have calculated the variation of the radiation balance of the thickness of the atmosphere of the influx

$$\Delta F_a = \Delta F(\infty) - \Delta F(0). \quad (11)$$

For the sake of comparison, appropriate variations of balances for long-wave radiation are listed in Table 6.7.

Table 6.7. Variations of the radiation balance of the upper boundary of the atmosphere ($\Delta F(\infty)$), the surface ($\Delta F(0)$) and the influx to the atmosphere's thickness (ΔF_a) in the event of cirrus clouds as compared with the cloudless atmosphere; corresponding variations of the long-wave radiation balance ΔF^{therm} in $\frac{W}{m^2}$.

Date	Moscow time	τ	$m_v, g/cm^2$	Optical cloud model	$\Delta F(\infty)$		$\Delta F(0)$		ΔF_a		thermal		
					$r_{\theta} = 0.1$	$r_{\theta} = 0.2$	$r_{\theta} = 0.1$	$r_{\theta} = 0.2$	$r_{\theta} = 0.1$	$r_{\theta} = 0.2$	$\Delta F(\infty)$	$\Delta F(0)$	ΔF_a
19.V.87	17.30-18	0.33	1.3	I	15	18	-5	-3	20	21	30	12	18
				IV	-4	-3	-32	-25	28	28			
				III	-9	-4	-24	-19	15	15			
				II	18	23	-16	-13	34	36			
20.V.87	11.30-12	0.17	1.9	I	14	16	-2	-2	16	18	20	6	14
				IV	4	8	-18	-15	22	23			
				III	1	5	-13	-10	14	15			
				II	16	19	-7	-7	23	26			
22.V.87	13.30-14	0.46	2.8	I	14	19	-11	-6	25	25	29	11	18
				IV	-11	-1	-50	-42	39	41			
				III	-18	-9	-38	-29	20	20			
				II	18	25	-24	-21	42	46			

$$\begin{aligned} \Delta F^{therm}(\infty) &= -F_{\uparrow}(\infty) \\ \Delta F^{therm}(0) &= F_{\downarrow}(0) - F_{\uparrow}(0) \\ F_a^{therm} &= F^{therm}(\infty) - F^{therm}(0) \end{aligned} \quad (12)$$

As is evident from Table 6.7, already when clouds were of the optical thickness $\tau \approx 0.5$ (with due account of the non-spherical character of particles), we obtained a reduction of the radiation balance of the upper boundary of the atmosphere as compared with the clear atmosphere by the value of up to $18 W m^{-2}$ ($\Delta F(\infty) = -18 W m^{-2}$). Hence, despite the weakening of the long-wave cooling by clouds, the radiation heating of the system decreases due to the stronger reflection of solar radiation. For models of spherical particles an increase of the balance $F(\infty)$ by the value $14 - 25 W m^{-2}$ was obtained.

The variations of the influx to the atmosphere's thickness are always positive and almost do not depend on r_s , assumed in calculations. The influx can be both positive and negative. Close values ΔF_a for models I and III (the same as for models II and IV) mean that the main influence on the influx is exerted not by the shape of particles, but by the absorption of ice by substance, i.e. the parameter ω_2 determined from the sizes of particles. Variations of the radiation balance of the surface have a negative sign, i.e. in the daytime the surface becomes colder due to cirrus clouds despite the decrease of the cooling of the atmosphere by thermal radiation. (See $\Delta F^{therm}(0)$).

The studies performed refer to the specific middle-latitude region, daytime and spring-summer season. The calculations have shown the considerable sensitivity of the radiation regime in the event of cirrus clouds to the chosen optical model of the cloud. To specify the estimates obtained, it is necessary to have detailed experimental data on the distribution of cloud particles as far as their size, shape and optical characteristics are concerned.

Chapter 7

CONCLUSION

The month of May was chosen for the experiment relying on many years' observations of clouds at the Moscow University Meteorological Station in Moscow.

The state of the sky during the experiment conducted for two years in May was the following: from the overall number of cases of cloudiness C_i were presented in 40%. In 37% of cases of their availability other clouds were not observed. These estimates agree quite well with the data of Table 7.1 from (Hahn, C., *et al.*, 1984) where the global distribution of C_i during seasons over dry land and the ocean is shown on the basis of ground visual observations.

Table 7.1

	Winter	Spring	Summer	Autumn
1	46/30	47/32	41/31	42/31
2	45/9	41/10	33/9	38/9

Line 1 in the table is the per cent of the availability of C_i among all clouds under observation. Line 2 is the per cent of the absence of other types of clouds with the existence of C_i . The numerator refers to observations over dry land, the denominator to observations above the ocean.

It is seen that even in the event of the global averaging spring is the predominant period for observations.

According to aircraft observations in the Moscow Region (Baranov, A. A., 1964) the formation of C_i in 80% of cases is linked with atmospheric fronts - mostly with warm

fronts rather than with cold fronts and mostly in a warm season rather than in a cold season. Cirrus clouds emerge at a distance of about 800 km before the surface front. They are thin and are visible from the surface. With the approach to the front line the clouds become thicker and ever more frequently lie lower.

The question arises: what do we study in the ground-based experiment?

We study thin cirrus clouds more frequently than thick clouds (geometrically and optically). This is confirmed by the results of chapters 1-3. It is reasonable to study thin clouds for several reasons.

1. Thin clouds over the underlying surface with a small albedo (0.1 - 0.2 in spring in the region of the experiment) have a greater effect on the albedo of the system than dense clouds which lie over a surface with a great albedo, for instance, clouds lying below.
2. The variable greenhouse effect is created precisely by thin clouds. When $\tau > 2$ the cloud becomes absolutely black and, correspondingly, radiation from boundaries is determined only by temperature.
3. Thin clouds are poorly detected from satellites.

The purpose of the study was to determine the effect of cirrus clouds on integral (by the spectrum of wavelengths and by the directions) fluxes of solar and thermal radiation in order to introduce the results into the theory of the climate, into numerical models of the theory of the climate and into weather forecasts.

REFERENCES

- Abakumova, G. N., I. N., Plankhina, and T. A. Tarasova: The estimate of the aerosol optical thickness of the atmosphere from the data of ground-based and ship-based actinometry (comparison of various techniques). *Meteorologiya i Gidrologiya (in press)*.
- Anikin, P., A. I. Chavro, and A. Kh. Shukurov, 1981: A complex optical installation for studying the spectral transmission of the atmosphere on oblique and horizontal routes in the ultraviolet, visible and infrared spectral ranges (0.3-25 mcm). *The Physical Aspects of the Remote Sensing of the Ocean-Atmosphere System*, Moscow, Nauka Publishers, (In Russian).
- Asano, S., 1983: Light scattering by horizontally oriented spheroidal particles. *Appl. Opt.*, **22**, 1390-1396.
- Baranov, A. A., 1964: Frontal clouds and conditions of flights in them. Leningrad, Gidrometeoizdat Publishing House, 240 pp, (In Russian).
- Collection "Radiative properties of cirrus clouds." Nauka Publishers, 1989 (In Russian).
- Davis, P. A., W. A. Viezee, 1964: A model for computing infrared transmission through atmospheric water vapor and carbon dioxide. *J. Geophys. Res.*, No. 18, **69**.
- Feigelson, E. M., 1973: Radiant heat transfer in a cloudy atmosphere. Translated from Russian. NOAA by IPST, 191 pp.
- Feigelson, E. M., 1988: Fluxes of infrared thermal radiation in cirrus clouds. *Izvestiya Akademii Nauk SSSR. FAO series*, No. 8 **24**, 586-594.
- Gorchakova, I. A., 1989: Estimates of the errors of semi-black approximation. *Izvestiya Akademii Nauk SSSR. FAO series*, No. 1 **25**.
- Gorelik, A. G., L. S. Raikova, Yu. A. Frolov, 1975: Super-high-frequency radiometric methods of measuring moisture in the lower troposphere. *Meteorologiya i Gidrologiya*, No. 5, 106-112.
- Haun, C. J., *et al.*, 1984: Atlas of simultaneous occurrence of different cloud types over land. NCAR Technical Note T 241 STR, Boulder Company, 21 and 188 maps.
- Heymsfield, A. J., 1975a: Cirrus uncinus generating cells and the evolution of cirroform clouds. Part I: Aircraft observations of the growth of the ice phase. *J. Atmos. Sci.*, **32**, 798-808.
- Irwine, W. W. and J. B. Pollack, 1968: Infrared optical properties of water and ice spheres. *Icarus*, **8**, 321-360.
- Joseph, J. H., W. J. Wiscombe, and J. A. Weinman, 1976: The Delta-Eddington approximation for radiative flux transfer. *J. Atmos. Sci.*, **33**, 2452-2459.
- Kerker, M., 1969: *The scattering of light and other electromagnetic radiation*. New York-London, Academic Press, 645 pp.
- Kondratyev, K. Ya., 1960: The spectral albedo of natural underlying surfaces. *Meteorologiya i Gidrologiya*, 46-53.
- Liou, K.-N., 1973: Transfer of solar irradiance through cirrus cloud layers. *J. Geophys. Res.*, **78**, 1409-1418.
- Liou, K.-N., and G. D. Wittman, 1979: Parameterization of radiative properties of clouds. *J. Atmos. Sci.*, **36**, 1261-1273.
- Liou, K.-N., 1986: Influence of cirrus clouds on weather and climate processes: a global perspective. *Mon. Wea. Rev.*, **114**, 1167-1199.

- Liou, K.-N., 1975: On the transfer of solar radiation in aerosol atmosphere. *J. Atmos. Sci.*, **32**, 1166-1177.
- McClatchey, R. A. *et al.*, 1972: Optical properties of the atmosphere (third edition), AFCRL-72-0497, 108 pp.
- Nijlisk, H. J., and L. E. Samuel, 1969: The integral transmission function of the atmosphere for calculating the thermal radiation field in the troposphere. Collection "Tables of Atmospheric Radiative Properties." The Academy of Sciences of the Estonian SSR. Institute of Physics and Astronomy, Tartu, 128- 180, (In Russian).
- Pavlova, L. N., A. G. Petrushin, and T. A. Tarasova, 1981: Radiation properties of ice clouds. *Izvestiya Akademii Nauk SSSR*, FAO series, No. 4, 437-439.
- Plass, G. N., and G. W. Kattawar, 1971: Radiative transfer in water and ice clouds in the visible and infrared region. *Appl. Opt.*, **10**, 738- 748.
- Platt, C. M. R., and G. L. Stephens, 1980: The interpretation of remotely sensed high cloud emittances. *J. Atmos. Sci.*, **37**, 2314-2322.
- Platt, C. M. R., J. C. Scott, and A. C. Dille, 1987: Remote sounding of high clouds: Part VI: optical properties of midlatitude and tropical cirrus. *J. Atmos. Sci.*, **44**, 729-747.
- Pruppacher, H. R., and J. D. Klett, 1978: *Microphysics of Clouds and Precipitation*. 714 pp. D. Riedel Publishing Company.
- Sassen, K., 1978: Backscattering cross sections for hydrometeors: Measurements at 6328 Å. *Appl. Opt.*, No. 5, **17**, 804-806.
- Sassen, K., 1981: Infrared (10.6 μm) scattering and extinction in laboratory water and ice clouds. *Appl. Opt.*, **20**, 185-193.
- Tarasova, T. A., and E. M. Feigelson, 1981: On taking into account the effect of aerosol in radiant heat transfer. *Izvestiya Akademii Nauk SSSR*, FAO series, No. 1, **17**, 18-25.
- Van de Hulst, 1957: *Light scattering by small particles*. Willey, New York, 536 pp.
- Volkovitsky, O. A., L. N. Pavlova,, and A. G. Petrushin, 1984: *Optical properties of crystalline clouds*. Leningrad, Gidrometeoizdat Publishing House, 198 pp. (In Russian).
- Welch, R., S. K. Cox, and J. M. Davis, 1980: Solar radiation and clouds. *Meteorological Monographs* No. 39, **17**, 96 pp.
- Wendling, P., R. Wendling, and H. K. Weickmann, 1979: Scattering of solar radiation by hexagonal ice crystals. *Appl. Opt.*, No. 15, **18**, 2663-2671.
- World Climate Programme, WCP-55 Reports of the experts meeting on aerosols and their climatic effects, WMP, Dec. 1983.
- World Climate Research Programme, No. 7, WMO/TD, No. 149, October 1986, 140 pp.
- Zaitseva, N. A., and E. M. Feigelson, 1979: Specific features of radiant heat transfer in the tropics as inferred from the data of actinometric radio sounding in the TROPEX-74 expedition. *Izvestiya Akademii Nauk SSSR*, FAO series, No. 2, **15**.
- Zhuravlyova, V. A., S. F. Kalachinsky, and O. K. Kostko, 1983: Joint IR- radiometric and lidar studies of radiation characteristics of cirrus clouds. *Izvestiya Akademii Nauk SSSR, Fizika Atmosfery i Okeana (Physics of the Atmosphere and the Ocean)*, **19** 1167-1171.
- Zuyev, V. Ye., G. M. Krekov, M. Krekova, and I. E. Naats, 1976: Theoretical aspects of the problem of the laser sounding of clouds. *Problems of the Laser Sounding of the Atmosphere*. Novosibirsk, Nauka Publishers, (In Russian).